Chapter 8

Lateral Transport in the Ocean Interior

B. Fox-Kemper*, R. Lumpkin‡ and F.O. Bryan§

*Geological Sciences, Brown University, Providence, Rhode Island, USA

‡Physical Oceanography Division, Atlantic Oceanographic and Meteorological Laboratory, Miami, Florida, USA

§National Center for Atmospheric Research, Boulder, Colorado, USA

Chapter Outline

1. INTRODUCTION

The motions of the oceans span a vast range of length and time scales, consistent with the broad range of forcing from small and fast (wind gusts), large and fast (tides, diurnal cycle) to small and slow (coastal erosion), to large and slow (Milankovich and tectonic change). However, even forcing over a narrow band of space and time scales does not result in a narrow banded response, as nonlinear processes connect different scales and hydrodynamic instabilities produce new scales that differ from those of the forcing.

High-resolution models, satellites, and drifter observations generally agree about the surface signature of the mean and mesoscale motions of the surface ocean. Even coarse-resolution models approximate many nonlinear effects, such as the formation of the advective thermocline, meridional overturning circulations, and western boundary currents. However, the instabilities and small-scale processes that produce transient mesoscale and smaller motions are still not resolved routinely in global scale simulations, which is likely to be true for a few decades to come. Continued study of mesoscale processes and their parameterization will provide increasingly accurate understanding and models. This chapter focuses on the present understanding and remaining questions about the effect of these processes on the larger, steadier oceanic "general circulation."

Precise usage of "general circulation" is rarely exercised; it usually refers to a circulation governed by steady or simplified equations or observations that somehow reduce variability. Before computers, general circulation usually meant assuming steady, linear, strongly diffusive equations. Since computers, we refer to "general circulation models" or GCMs, that are too coarse to resolve some phenomena. Whatever is not resolved, apparently, is not part of the "general circulation." Now that we can afford to simulate all of the globe, GCM is sometimes taken as "global circulation model" or "global climate model" where

Ocean Circulation and Climate, Vol. 103, http://dx.doi.org/10.1016/B978-0-12-391851-2.00008-8

"circulation" and "climate" apparently are that which is resolved and everything else is not.

General circulation models have parameterizations to approximate all phenomena smaller or faster than the model can resolve directly. Which phenomena need to be parameterized depends on the model resolution and an assessment of the phenomena that dominate that scale. The emphasis here is on the present global ocean models, which have a resolution too coarse to directly resolve features that are a few hundred kilometers in the horizontal or smaller. Model resolution has increased steadily with computing power and so the definition of general circulation grows to include more phenomena but direct solution of the Navier–Stokes equations for the global ocean is still centuries away, based on current trends. So, parameterizations of some unresolved ocean phenomena will remain part of oceanography for the foreseeable future. Mesoscale and smaller processes transport tracers, momentum, and energy, and these transports constitute a non-negligible contribution to the global ocean's general circulation and stratification.

This chapter reviews principles behind the processes that dominate the lateral transport of fluid properties: the general circulation and mesoscale eddies. Away from the surface, both general circulation and eddies are thought to be nearly conservative in many properties. The conservation principles, and how they are formulated into guiding principles for the development of parameterizations, constitutes the first few sections. A brief discussion of the interactions between the unresolved and resolved processes follows. Later sections present high-resolution numerical and observational evidence to illustrate some parameterization principles in present practice and suggest future improvements.

2. THEORY OF MASS, TRACER, AND VECTOR TRANSPORT

This section contains an introduction to the relevant equations of fluid motion in the forms most useful for the discussion of transport processes to come in later sections. The compressible equations with a generic equation of state are a useful starting point. They are contrasted against the "primitive" equations usually simulated in ocean models, both in depth-coordinate and density-coordinate versions. Care is taken with the connections between energy and buoyant restoring force. The importance of the vertical coordinate, averaging operations, and relevant "eddy" correlations are also discussed in preparation for later sections.

2.1. Fundamental Equations

The general equations of motion for a rotating, stratified fluid are the rotating Navier–Stokes equations, combined with the first and second laws of thermodynamics. With appropriate initial and boundary conditions, density (ρ), absolute pressure (P), three velocity components $\left(\overline{u}\right)$, specific internal energy (e), specific entropy (s), salinity (S) and passive tracer (c) in mass fraction units may be determined using these equations and standard thermodynamic relations (e.g., Vallis, 2006).

The fundamental continuity and tracer conservation equations for a compressible fluid is used later and so are given here:

$$\frac{\partial \rho}{\partial t}+\nabla_i(\rho u_i)=0, \quad \frac{\partial \rho c}{\partial t}+\nabla_i(\rho u_i c)=\rho \dot{c}. \tag{8.1}$$

For consistency with later sections where tensor notation is more convenient, Cartesian tensors are used throughout as also Einstein summation (repeated indices indicate summation over all coordinates). For example $\nabla_i(\rho u_i) \equiv \frac{\partial \rho u}{\partial x}+\frac{\partial \rho v}{\partial y}+\frac{\partial \rho w}{\partial z}$, and $u_i u_i \equiv u_j u_j \equiv u^2+v^2+w^2$. The ∇ operator with a subscript denotes partial differentiation in that direction. Griffies (2004) has a thorough discussion on using tensor notation for ocean modeling. The dot above c indicates rate of change of concentration due to non-reversible or non-conservative effects such as sources, sinks, and diffusion. Cartesian coordinates and flux form equations (where each tendency may be balanced against the divergence of a flux) are used. The flux form helps to compare transport among different equation sets to come. The equations can easily be converted to curvilinear or spherical coordinates with the metric tensor formalism described in Griffies (2004); some care is required to maintain the flux-conservation principles. For motions that span only a fraction of the earth's circumference, such as a single model grid point where a parameterization may apply, these equations are sufficient and accurate to describe the tangent plane to the spherical earth at that location.

2.1.1. Primitive Equations

Present large-scale ocean models do not solve the Navier-Stokes and thermodynamic equations, which have unwanted complexity, such as a time step limited by the speed of sound. Instead, the Boussinesq, hydrostatic, traditional, and geopotential simplification approximations are typical (Griffies and Adcroft, 2008; Young, 2010; Chapter 20) although exceptions exist (e.g., McDougall et al., 2002; Mahadevan, 2006). The hydrostatic approximation $\nabla_z P=-\rho g$ is appropriate for large-aspect-ratio flow, and the background pressure ($P_0-\rho_0 g z$) is hydrostatic, but the hydrostatic approximation will not be made to the vertical momentum equation so that the symmetries are more apparent.

$$\nabla_i u_i=0, \quad b=\tilde{b}(S,\Theta,P_0-\rho_0 g z), \tag{8}$$

$$\frac{\partial S}{\partial t}+\nabla_i(u_i S)=\dot{S}, \quad \frac{\partial c}{\partial t}+\nabla_i(u_i c)=\dot{c}, \quad \frac{\partial}{\partial t}\Theta+\nabla_i(u_i \Theta)= \tag{8}$$

$$\frac{\partial u_j}{\partial t} + \int_{j:k} f u_k + \nabla_j (u_j u_j) + \nabla_j p - b\delta_{z:j} = \dot{u}_j, \qquad (8.4)$$

where the buoyancy is $b = \lg(\rho_0 - \rho)/\rho_0$,[1] the dynamic pressure is $p = (P - P_0)/\rho_0 + gz$, and the constant background values are ρ_0 for density and $P_0(x, y, t)$ for pressure variations due to the sea surface height or atmosphere. When the coordinate names x, y, z appear as indices, for example, $\epsilon_{j:k}$, only that component in the x (zonal), y (meridional), or z (vertical) direction is intended. For example, the vertical velocity is $w = u_z$. Tildes denote thermodynamic relations $\left(\text{e.g., } \tilde{b}(S, \Theta, P_0 - \rho_0 gz)\right)$[2] as opposed to values (e.g., b). Conservative forces (gravity and centrifugal) are represented by an averaged value of gravitational acceleration (g) and deviations from the local geoid (z). Nonconservative forces ($\dot{u}$), heating, and irreversible and diffusive processes ($\dot{S}$, $\dot{\Theta}$, $\dot{c}$) are included but not specified. The traditional approximation reduces the directionality of the Coriolis force based on the axis of planetary rotation (Ω) to the local vertical component f. The Kronecker δ and Levi–Civita totally antisymmetric symbol (ϵ) are needed to provide the direction of the Coriolis and buoyancy forces.[3]

The temperature variable Θ can be ordinary temperature, potential temperature, or conservative temperature to have (Equation 8.3) represent seawater thermodynamics with increasing accuracy (McDougall, 2003; Nycander, 2011; Young, 2010; Chapter 6). Near-surface forcing by the sun and infrared radiation can be accounted for via $\dot{\Theta} = \dot{e}/c_p^0$. Latent and sensible heat exchange with the atmosphere, evaporation and precipitation, and turbulent boundary layer mixing also contribute to the right sides ($\dot{u}$, $\dot{S}$, $\dot{c}$, $\dot{\Theta}$). Away from the boundaries, the right sides of Equation (8.3) are generally very small. Thus, water mass analysis can detect where waters were "formed" after decades or centuries of advection and weak diffusion. The mixing processes that do contribute to nonzero right sides of Equation (8.3), along with their sources and rates, are reviewed in Chapter 7.

Boussinesq models have no conversion of internal energy to mechanical energy, but do allow conversion between potential and kinetic energy via sinking of dense water or rising of light water via wb (Young, 2010). The Boussinesq energy equations are

$$\frac{\partial}{\partial t}\frac{u_j u_j}{2} + \nabla_i u_i \left(\frac{u_j u_j}{2} + p\right) - wb = u_j \dot{u}_j, \quad \frac{\partial}{\partial t} h^{\ddagger} + \nabla_i u_i h^{\ddagger} + wb = \frac{\partial \tilde{h}^{\ddagger}}{\partial \Theta}\dot{\Theta} + \frac{\partial \tilde{h}^{\ddagger}}{\partial S}\dot{S}, \qquad (8.5)$$

$$\text{where } \tilde{h}^{\ddagger} \equiv \int_Z^0 \tilde{b}(S, \Theta, P_0 - \rho_0 gz')\mathrm{d}z'. \qquad (8.6)$$

The enthalpy (and the Boussinesq dynamic enthalpy $h^{\ddagger}$) is a key thermodynamic variable because it is very nearly conserved during mixing (Young, 2010; chapter 6). In a stably-stratified ocean, wb keeps water parcels near a fixed location. The restoring force for internal waves (where $wb < 0$) is a good example. A second important role for wb is as the source of energy for baroclinic instabilities, which convert mean potential energy to eddy energy by correlating eddy motions with water buoyancy (thus $wb > 0$ on average). Likewise, unstable density profiles convect with $wb > 0$.

2.1.2. Minimal-Disturbance Planes and Slopes

In a stratified ocean, arbitrary adiabatic displacement of a water parcel typically results in a buoyancy anomaly and force that act to restore or destabilize the parcel. One direction will generally maximize this effect and motions in a plane perpendicular to this direction will minimize it. Potential density or buoyancy b, neutral density (McDougall, 1987), and the Boussinesq dynamic enthalpy, $\tilde{h}^{\ddagger}$ in Equation (8.5) above (Young, 2010; Nycander, 2011) are thermodynamic variables that can be used to estimate the direction in which displacements create maximal disturbances of stratification or energy. The "diapycnal" direction ($\mathcal{D}_i$), the "dianeutral" direction ($\mathcal{N}_i$), and the "P vector" ($\mathcal{P}_i$) are all maximal-disturbance directions given by

$$\mathcal{D}_i = \nabla_i b, \quad \mathcal{N}_i = \left(\frac{\partial \tilde{b}}{\partial \Theta}\right)_{S,z} \nabla_i \Theta + \left(\frac{\partial \tilde{b}}{\partial S}\right)_{\Theta,z} \nabla_i S,$$

$$\mathcal{P}_i = \left(\frac{\partial \tilde{h}^{\ddagger}}{\partial \Theta}\right)_{S,z} \nabla_i \Theta + \left(\frac{\partial \tilde{h}^{\ddagger}}{\partial S}\right)_{\Theta,z} \nabla_i S,$$

Each estimates a direction for maximum effect by displacement or mixing. Displacements in the perpendicular plane result in a minimal disturbance. Large scale oceanic motions are generally believed to be dominantly oriented along a minimal-disturbance plane. At different levels of thermodynamic accuracy, these planes are generally called "isopycnals" (with potential density implied), "neutral planes," or "P planes." They are not equal or exactly parallel, and only the simplest, least accurate case $\mathcal{D}_i$ can be thought of as determined by a global surface (isopycnals, where potential density and b are constant). No unique surface or thermodynamic variable connects all the local neutral planes

1. Young (2010) uses a different form that is slightly simpler thermodynamically but asymptotically identical.
2. As noted by Vallis (2006) and Young (2010). $P_0 - \rho_0 gz$ is the approximation to thermodynamic pressure appropriate for energetically consistent Boussinesq equations. So this thermodynamic relation gives buoyancy as a function of salinity, temperature, and pressure.
3. The traditional approximation is best justified when accompanied by the hydrostatic approximation. It can be relaxed, with some added complications (Sheremet, 2004).

or local P planes into global surfaces. However, a minimal-disturbance slope can always be calculated locally using $\mathcal{S}_\gamma = -\mathcal{D}_\gamma/\mathcal{D}_z$, $\mathcal{S}_\gamma = -\mathcal{N}_\gamma/\mathcal{N}_z$, $\mathcal{S}_\gamma = -\mathcal{P}_\gamma/\mathcal{P}_z$, or similar approximations with corresponding levels of thermodynamic sophistication. Greek indices, for example, γ, indicate throughout that the index is to vary only over the horizontal directions, that is, x and y. Depending on this level of sophistication, different terms are used to describe the fluxes in different directions: skew, isopycnal, and diapycnal (buoyancy); adiabatic and diabatic (energy); isentropic and irreversible (entropy); epineutral and dianeutral (neutral planes). Here, we use minimal-disturbance plane and maximal-disturbance direction to apply generally.

2.1.3. Density-Coordinate Continuity and Tracer Equations

Since lateral motions are thought to be oriented along the minimal-disturbance plane, a density-like variable that approximates this slope globally—usually potential density or buoyancy—is often used as a vertical coordinate in models. If these surfaces are not too steep, then the hydrostatic approximation is valid and the conservation laws for volume and tracer may be written for this density-coordinate model as (McDougall and Dewar, 1998; Hallberg, 2000):

$$\frac{\partial h}{\partial t} + \nabla_\gamma \cdot h u_\gamma = -\frac{\partial}{\partial \varrho}\left(h \frac{D\varrho}{Dt}\right) \equiv -\frac{\partial w_e}{\partial \varrho}, \quad \frac{\partial}{\partial t}(hc) + \nabla_\gamma \cdot h u_\gamma c = \frac{\partial F_c}{\partial \varrho} - \frac{\partial w_e c}{\partial \varrho}. \tag{8.7}$$

The change in height with ϱ is $h \equiv -\rho_0 z_\varrho$. Note that the precise meaning of "horizontal" and "vertical" holds some complexity in density-coordinate models; Young (2012) offers much to clarify.

If ϱ is materially conserved, then the entrainment velocity (w_e) vanishes, and these equations are formally identical to the *compressible* mass conservation and tracer equations (Equation 8.1), with "layer thickness" (h) in place of fluid density (ρ). A crucial element of modern eddy parameterizations results from idealizing their transport as flowing along 2D compressible, minimal-disturbance surfaces. They are thus assumed to inhabit only a subset of the possible motions in the 3D nearly-incompressible flow governed by the Boussinesq equations. The formal connection between Equations (8.7) and (8.1) is useful when considering how to parameterize the effects of eddy stirring (Dukowicz and Smith, 1997).

2.2. Steady, Conservative Equations

The oceanic "general circulation" is often intended to imply a purely steady $\left(\frac{\partial}{\partial t} = 0\right)$ or time-mean $\left(\frac{\partial}{\partial t} \approx 0\right)$ solution to the primitive equations or approximations thereof. For steady, conservative flow, time-derivatives and the non-conservative terms on the right side of Equations (8.3)–(8.5) are neglected. A total specific energy, or Bernoulli function, can be found by eliminating wb between the equations in Equation (8.5). These simplifications yield properties that are conserved in the direction of flow.

$$u_i \nabla_i S = 0, \quad u_i \nabla_i \Theta = 0, \quad u_i \nabla_i \left(\frac{u_j u_j}{2} + p + h^\ddagger\right) = 0, \tag{8.8}$$

$$u_i \nabla_i Q(\vartheta) \equiv u_i \nabla_i \left(\left[\epsilon_{jkl} \nabla_k u_l + 2\Omega_j\right] \nabla_j \vartheta\right) = \frac{\partial \vartheta}{\partial x}\frac{\partial b}{\partial y} - \frac{\partial \vartheta}{\partial y}\frac{\partial b}{\partial x}. \tag{8.9}$$

In Equation (8.8), gradients of salinity, conservative temperature, and Bernoulli function must all be perpendicular to the direction of steady motion. The Ertel potential vorticity $Q(\vartheta)$, based on a materially conserved tracer ϑ, will itself be materially conserved if the buoyancy is zero or ϑ and b are functionally related at each depth. In either case, the right side of Equation (8.9) vanishes. For example, if $\vartheta = \Theta$ and S is constant at that level, then $Q(\Theta)$ is conserved. Most often, $Q(b)$ is used, as b is a conserved tracer if the thermodynamic equation of state can be approximated and combined using Equation (8.8) (e.g., by a local linearization of $\widetilde{b}$).

According to Equation (8.8), conservative, steady flow proceeds in such a way that salinity, conservative temperature, buoyancy, potential vorticity, and Bernoulli function are all constant along streamlines. Many successful theories for steady oceanic flows result (e.g., Sverdrup, 1947; Charney, 1955; Welander, 1959; Stommel and Arons, 1960; Stommel and Schott, 1977; Luyten et al., 1983; Rhines, 1986). These steady solutions are the quantitative basis of understanding for the oceanic gyres, meridional overturning circulation, and generally the oceanic conveyor (Broecker, 1987), as well as air mass analysis (reviewed by Hoskins et al., 1985), and water mass analysis (e.g., Talley and McCartney, 1982; Levitus et al., 1993). These conservative, steady methods can often be adapted to weak diffusion (Welander, 1971; Rhines and Young, 1982; Haynes and McIntyre, 1987; Samelson and Vallis, 1997) and identification of related water masses over long distances, respecting the nonlinear equation of state (McDougall and Jackett, 2007; McDougall and Klocker, 2010).

Now we turn to another aspect of an understanding of the general circulation—how the large-scale, time—mean flow differs from the steady flow, which involves the averaged effects of mesoscale eddies and other smaller variability on the general circulation.

2.3. Reynolds-Averaged Equations

The ocean is not steady, nor is it adiabatic, isentropic, or inviscid. The remainder of this chapter focuses on the

unsteady behavior, in particular the contribution from unsteady $O(100\text{ km}, 10\text{ day})$ mesoscale ocean eddies. Diabatic and irreversible effects and mixing are discussed in Chapter 7. Here, all unsteady mesoscale motions are called eddies.

The study of eddy effects on the general circulation began soon after the Mid-Ocean Dynamics Experiment (MODE) (e.g., Holland and Lin, 1975; McWilliams and Flierl, 1976) and fundamental understanding soon followed (Rhines and Holland, 1979; Holland and Rhines, 1980; Rhines and Young, 1982). Eddies play a leading order role in the overturning of the Antarctic Circumpolar Current (Johnson and Bryden, 1989; Henning and Vallis, 2005; Radko and Marshall, 2006), while others have explained the effects of eddies on the gyres (Scott and Straub, 1998; Berloff and McWilliams, 1999; Fox-Kemper and Pedlosky, 2004; Henning and Vallis, 2004; Radko and Marshall, 2004; Fox-Kemper, 2005; Fox-Kemper and Ferrari, 2009). At depth, eddy-induced tracer transport usually exceeds the Eulerian mean transport (Rhines and Holland, 1979; Lozier, 1997, 2010). In western boundary currents, two-way interaction is possible between the time–mean flow and the eddies (Pedlosky, 1984; Edwards and Pedlosky, 1998; Jochum and Malanotte-Rizzoli, 2003; Fox-Kemper, 2004; Fox-Kemper and Ferrari, 2009; Grooms et al., 2011), and the recirculation gyres nearby (Nurser, 1988; Fox-Kemper and Pedlosky, 2004; Kravtsov et al., 2006; Waterman and Jayne, 2011). Eddies can connect basins where mean currents cannot (Gordon et al., 1992; Hallberg and Gnanadesikan, 2006). Numerical studies of oceanic eddies are numerous, and recently even coupled climate models have been run with partially resolved eddies (McClean et al., 2011; Delworth et al., 2012). However, it is likely that parameterization of eddy effects will continue for some decades in centennial-scale climate simulations and high-complexity (e.g., biogeochemical) models. Analytic studies, in particular, benefit from good approximations of eddy effects on the general circulation (Radko and Marshall, 2006; Fox-Kemper and Ferrari, 2009; Smith and Marshall, 2009; Grooms et al., 2011).

Early inclusion of eddies took the form of "eddy viscosity," where the viscosities are increased until nonconservative terms enter the dominant momentum balance (e.g., Munk, 1950; Parsons, 1969). Explicit physical, rather than numerical, discussion of eddy viscosity in coarse-resolution models are rare (Smith and McWilliams, 2003), although results are sensitive to the viscosity chosen (Jochum et al., 2008). Sometimes more complex effects of eddies can be treated as a viscosity (Johnson and Bryden, 1989; Fox-Kemper and Ferrari, 2009). However, all coarse-resolution models use either explicit eddy viscosity or numerical schemes that amount to the same. In eddy resolving models, choosing diffusivity and viscosity carefully allows cascades of energy and enstrophy and aids accuracy in boundary current separation (Smagorinsky, 1963; Leith, 1996; Griffies and Hallberg, 2000; Chassignet and Garraffo, 2001; Arbic et al., 2007; Bryan et al., 2007; Fox-Kemper and Menemenlis, 2008).

In modern coarse-resolution models, a combination of "eddy diffusivity" and "eddy-induced velocity" is typically used (Redi, 1982; Gent and McWilliams, 1990). One reason is that mesoscale eddies—at least baroclinic mesoscale eddies—appear in the large-scale momentum equation at lower order through redistribution of buoyancy and potential vorticity rather than directly through Reynolds stresses (Andrews and McIntyre, 1978b; Greatbatch and Lamb, 1990; Gent and McWilliams, 1996; Wardle and Marshall, 2000; Eden, 2010b; Grooms et al., 2011; Marshall et al., 2012). Further, eddy stresses that are not connected to buoyancy and potential vorticity transport are more difficult to parameterize and sometimes result in "negative viscosities" (e.g., Berloff, 2005), as the steady Bernoulli conservation law in Equation (8.8) does not result in a local time–mean balance.

Thus, it is the eddy transport of active and passive scalar tracers that is the primary focus of present coarse-resolution modeling effort and the remainder of this chapter. The time–mean, coarse-resolution equations can be written, returning to Cartesian coordinates, as

$$\nabla_i\left(\bar{u}_i\bar{S}+\overline{u_i'S'}\right)=\bar{\bar{S}},\quad \nabla_i\left(\bar{u}_i\bar{\Theta}+\overline{u_i'\Theta'}\right)=\bar{\bar{\Theta}},$$
$$\nabla_i\left(\bar{u}_i\overline{Q(b)}+\overline{u_i'Q(b)'}\right)\approx 0,\quad \nabla_i\left(\bar{u}_i\bar{c}+\overline{u_i'c'}\right)=\bar{\bar{c}}. \tag{8.10}$$

Here, overbars denote averaging to a coarse-resolution and slowly-varying in time, and primes denote mesoscale and submesoscale deviations from that mean.[4]

The fluxes appear entirely inside a divergence in Equation (8.10), which has led some authors to treat rotational eddy fluxes as less important (e.g., Marshall and Shutts, 1981; Bryan et al., 1999; Eden et al., 2007b). Often, it is suggested that removing or adjusting a rotational contribution will lead to fluxes that are more aligned with their corresponding gradient or more likely to yield positive diffusivities. The rotational change may be chosen broadly, as in a bounded domain rotational fluxes are not uniquely defined (Fox-Kemper et al., 2003). However, here eddy fluxes will be diagnosed both from drifters using observed trajectory anomalies from the time-mean flow and from a realistic model transporting passive tracers. These fluxes and diffusivities can be kinematically related to the theory of diffusion by continuous movements of Taylor (1921)—if their rotational parts are left unchanged. Changing the rotational fluxes violates this connection to fundamental fluid processes. Here fluxes will be

4. The averaging procedure is assumed to have the properties of a Reynolds-average, or $\overline{(\cdot)}=\overline{(\cdot)}$, $\overline{(\cdot)'}=0$, and $\overline{(*)(\cdot)'}=\overline{(*)}\,\overline{(\cdot)'}=0$.

related directly to an anisotropic diffusivity, which implies positive diffusivity nearly everywhere, natural boundary conditions, but at the cost of fluxes that are not necessarily down their mean gradient.

Even when the non-conservative terms on the right of Equation (8.10) are negligibly small in comparison to the advection terms on the left so that the flow is still "conservative," the eddy correlations on the left may still be as large as the mean tracer transport. Thus, the unsteady, conservative ocean solutions are potentially quite different from the steady, conservative oceanic solutions. Approaching the infinite Péclet limit requires some care, as even weak non-conservative terms may strongly affect the conservative fluxes (e.g., Jones and Young, 1994; Eden et al., 2007a), but the primary discussion of non-conservative mixing in this volume is found in Chapter 7.

Averaging the density-coordinate equations (Equation 8.7) is also useful. Often the averaging will be taken at a fixed density, which follows the displacement of the density surfaces and can make fewer explicit eddy correlations appear (de Szoeke and Bennett, 1993; Young, 2012). Weighting each average by thickness or treating hu as a unit (thickness-weighting) in the density-coordinate equations is equivalent to treating ρu_i as a unit (Hesselberg or Favre averaging) in the compressible fluid equations (Greatbatch and McDougall, 2003).

In the remainder of this chapter, estimates of the eddy properties, eddy fluxes, and eddy correlations in the Equation (8.10) will be presented. From data, the Lagrangian displacements of fluid parcels will be approximated from surface drifter trajectories. Assuming a scale separation between the background tracer gradients and the decorrelation length and assuming the properties of the fluid parcels are conserved over the decorrelation time, the tracer fluxes may be related to the parcel displacements. Some of the theory of Taylor (1921) is reviewed so that these results may be understood in relation to eddy diffusivity. Direct analysis of multiple tracers in high-resolution global ocean models is also presented. This method has been used before in simpler contexts to estimate the Lagrangian transports (Plumb and Mahlman, 1987; Bratseth, 1998). Finally, studies using satellite and *in situ* data together with turbulence or hydrodynamic stability theories are also refer to, to show that different approaches find similar results.

From Figure 8.1 one should expect fair consistency between the estimates. Shown are the mean and eddy kinetic energies of the drifters, model, and AVISO multi-satellite reconstruction. The model used is an improved version of the Maltrud and McClean (2005) global 0.1° POP model, with climatological "normal-year" forcing (Large and Yeager, 2004). Consistent with the conclusions of McClean et al. (2006), the model agrees with the AVISO altimetry. However, the drifter eddy kinetic energy is quite a bit larger in the eastern side of the subtropical and subpolar gyres than either the satellite geostrophic velocity or model total velocity indicates.[5] The higher drifter kinetic energy likely results from smaller mesoscale and submesoscale features that are not resolved *spatially* by either the satellite or model (Fratantoni, 2001; Capet et al., 2008; Lévy et al., 2010; Lumpkin and Elipot, 2010; Fox-Kemper et al., 2011).

2.4. Diffusion by Continuous Movements

Taylor (1921) successfully quantifies the effects of small-scale discrete and continuous motions of a fluid. A result of particular interest here is that while the root-mean-square (rms) of parcel displacements increases on integration over a time τ (first linearly, then as the square root), the covariance of parcel displacements and parcel velocities increases at first and then saturates after the decorrelation timescale, T, when the velocity autocorrelation following a parcel displacement goes to zero. After saturation, Lagrangian displacements Y' and Lagrangian velocities V' obey:

$$\overline{Y'(\tau)Y'(\tau)} \approx 2\overline{u'^2}\tau T, \quad \overline{Y'(\tau)V'(\tau)} \approx 2\overline{u'^2}T. \tag{8.11}$$

The constant velocity-displacement covariance can be interpreted as a form of eddy diffusivity for stationary, homogeneous turbulent flow.

This general approach can be extended in a stationary, homogeneous, incompressible, 3D flow (Batchelor, 1949; Monin et al., 2007, p. 542), by using the fluid parcel displacement covariance:

$$D_{ij}(\tau) = \overline{Y_i'(\tau)Y_j'(\tau)} = \int_{t_0}^{t_0+\tau}\int_{t_0}^{t_0+\tau} \overline{V_i'(x,t_1)V_j'(x,t_2)}\,\mathrm{d}t_1\mathrm{d}t_2. \tag{8.12}$$

The average (overbar) is an ensemble average over many displaced fluid parcels. For sufficiently long times $\tau \gg T_{ij}$, the covariance becomes linear in time (τ):

$$D_{ij}(\tau) \approx \sqrt{\overline{u_i'^2}\,\overline{u_j'^2}}\,T_{ij}\tau,$$

$$T_{ij} = \frac{\int_0^\infty \left(\overline{V_i'(x,s)V_j'(x,s)} + \overline{V_j'(x,s)V_i'(x,s)}\right)\mathrm{d}s}{\sqrt{\overline{u_i'^2}\,\overline{u_j'^2}}}. \tag{8.13}$$

No summation is implied on the repeated indices of D_{ij} and T_{ij}. Note that the Eulerian velocity scales u are used to estimate the size of the Lagrangian velocity correlations, consistent with homogeneous, stationary turbulence where these scales are closely related.

5. The drifter data is filtered to remove inertial motions (5-day lowpass), and the timescale of the filtering is similar to that used for the altimetry (7 days).

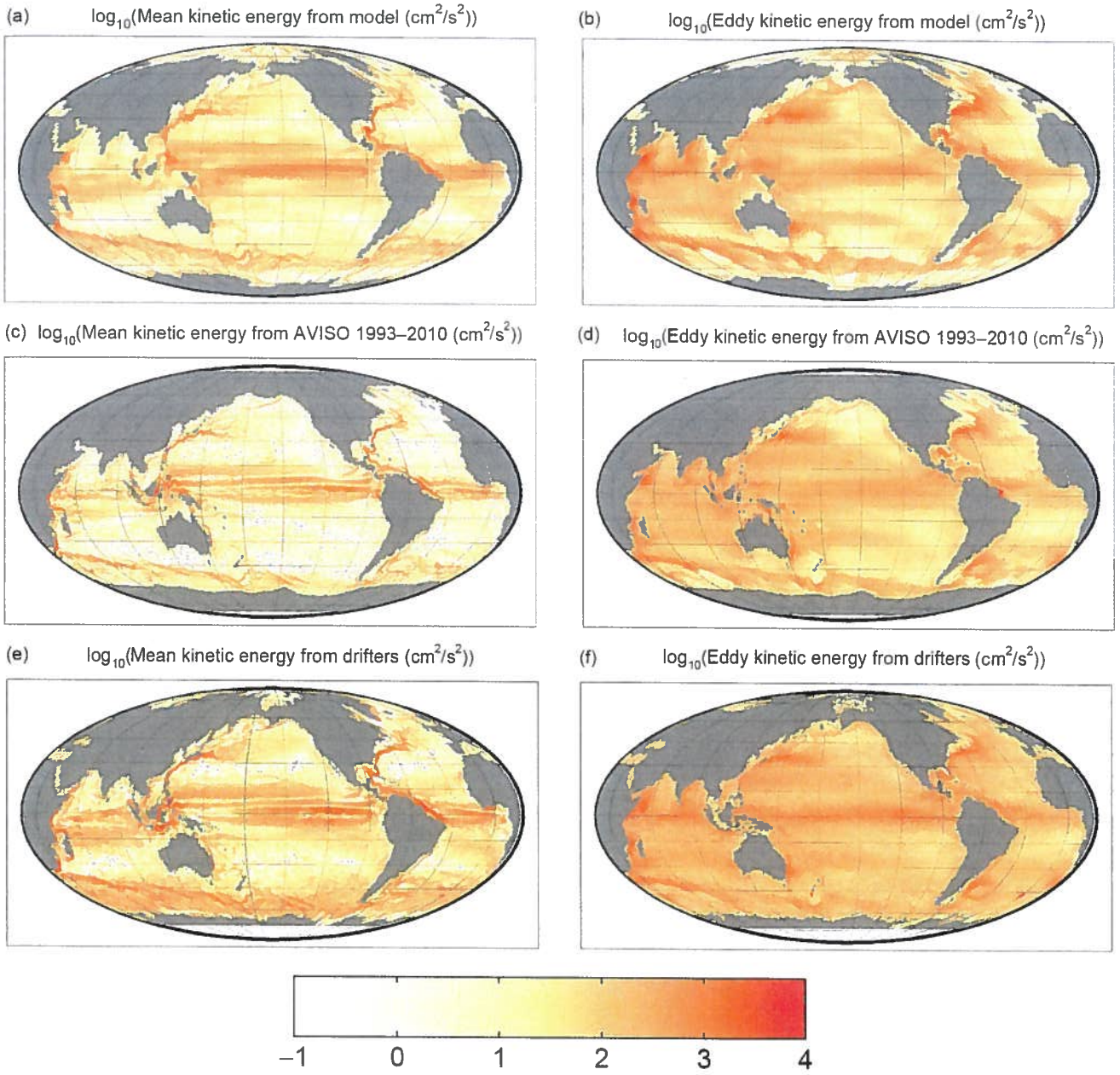

FIGURE 8.1 Mean (a, c, and e) and eddy (b, d, and f) kinetic energy from a global 0.1° model (see text for description), SSALTO/DUACS multi-satellite Maps of Absolute Dynamic Topography (MADT) product distributed by AVISO (c and d) which is based on weekly data, and from surface drifters (e and f; Lumpkin and Garraffo, 2005; Lumpkin and Garzoli, 2005), which are filtered to remove variability on timescales less than 5 days. Drifter mean kinetic energy is the energy in the time averaged flow while eddy kinetic energy is energy in motion with 5–7 day or longer timescales. Model mean kinetic energy is the energy of time-averaged flow, while eddy kinetic energy is the deviation from time-mean.

The proportionality with time of the displacement covariance for long times (τ) may be associated with an eddy diffusivity tensor, K_{ij}:

$$K_{ij} \approx \frac{1}{2}\sqrt{\overline{u_i'^2}\,\overline{u_j'^2}}\,T_{ij} = \frac{1}{2}\frac{\mathrm{d}D_{ij}(\tau)}{\mathrm{d}\tau} = \int_0^\infty \frac{1}{2}\left(\overline{V_i'(x,s)V_j'(x,s)} + \overline{V_j'(x,s)V_i'(x,s)}\right)\mathrm{d}s. \quad (8.14)$$

K_{ij} is symmetric by (8.14) and depends solely on the correlations of Lagrangian velocity displacements and velocity magnitudes in different directions. These velocities are likely to differ in each direction when symmetries are broken, for example by gravity, rotation, or other body forces. Similarly, the components of the decorrelation timescale T_{ij} are likely to vary if eddies tend to remain more coherent in one direction versus another, as is the case in an "eddy street" or turbulent wake. If a tracer is nearly conserved over the timescale T_{ij}, then every displaced fluid parcel carries its tracer with it, and the diffusivity K_{ij} may

be used to diffuse the average tracer concentration as $K_{ji}\nabla_i\bar{c} \approx -\overline{u'_j c'}$, or

$$\frac{\partial \bar{c}}{\partial t} + \nabla_i(\bar{c}\bar{u}_i) = \nabla_j\left(K_{ji}\nabla_i\bar{c}\right) + \bar{\dot{c}}, \tag{8.15}$$

where all averages are at a fixed depth (Eulerian).

2.4.1. Diagnosing Eigenvectors, Eigenvalues, and Principal Axes of Diffusivities

Any symmetric tensor can be fully described by its real eigenvalues and orthogonal eigenvectors. The equation that is satisfied by the ith eigenvalue $\lambda(i)$ and ith eigenvector $v(i)$ of a tensor M is:

$$M_{kl}v_l(i) = \lambda(i)v_k(i). \tag{8.16}$$

Thus, for that particular eigenvector $v(i)$, the action of matrix multiplication by the tensor is the same as multiplication by the *scalar* eigenvalue $\lambda(i)$. However, vectors not aligned with $v(i)$ acted upon by the tensor will *not* be likely to behave as though multiplied by a scalar. A 3×3 tensor has three eigenvectors and eigenvalues, and they are real for symmetric tensors. For real and symmetric tensors, the eigenvectors may always be chosen to be an orthonormal set, often called the *principal axes* of the tensor.

The (non-negative) eigenvalues of the diffusivity K_{ij} represent a typical value of the diffusivity in each of three different eigenvector directions. In the absence of a background flow, a tracer is diffused when its gradient is oriented partly along a principal axis. The component of the gradient will be reduced *down-gradient along that direction alone* by the associated eigenvalue (diffusivity). Thus, for a tracer whose gradient is oriented along an eigenvector, the diffusivity is effectively a scalar by Equation (8.16). However, it is uncommon for an arbitrary tracer gradient to align with a principal diffusivity axis. In this case, the tracer is diffused *anisotropically*, that is, at different rates along each principal axis simultaneously. Anisotropic diffusion results from a symmetric K with distinct eigenvalues.

Only isotropic, homogeneous turbulence with no background flow is likely to be represented well by a scalar diffusivity for arbitrary tracers (i.e., three equal eigenvalues). In this case, any gradient direction can be treated as an eigenvector direction and a scalar diffusivity can be used in place of K_{ij}. In a typical oceanic flow, the rms velocities and decorrelation times in Equation (8.14) differ in each direction. Even in isotropic, homogeneous turbulence, a background flow often leads to an anisotropic effective diffusivity (Taylor, 1953; Ferrari and Nikurashin, 2010).

Much confusion has arisen from apparently negative components of the diffusivity tensor in a realistic flow. Frenkiel (1952) shows examples of autocorrelation functions and the corresponding displacement covariances, and finds that rarely does the autocorrelation change sign frequently and vigorously, so the diagonal elements of D_{ij} are generally positive and only weakly related to the details of the autocorrelation shape. To put it another way, the diffusivity eigenvalues are generally likely to be positive. The trace of a tensor is not affected by rotation, including rotation into and out of the principal axis orientation. Thus, the sum of the diagonal elements tends to be positive in all coordinate systems. Indeed, the displacement covariance is most naturally measured in the principal axis coordinate system if known, as the tensor will be diagonal in that basis. In other coordinate systems, the elements may be positive or negative, which is not necessarily an indication of anti-diffusive behavior and negative eigenvalues, just an indication that the coordinate system is not aligned with the principal axes.

Eddy diffusivities must be positive in a sense found from the tracer variance equation, derived from Equations (8.3) and (8.10), to be

$$\frac{\partial \overline{c'^2}}{\partial t} + \nabla_i\left(\overline{u_i c'^2}\right) + \nabla_i\left(\overline{u'_i c'^2}\right) + 2\overline{u'_i c'}\nabla_i\bar{c} = \overline{\dot{c}'c'}. \tag{8.17}$$

The first two terms do not create variance, they just transport it materially with the mean flow. If the third, triple-correlation term is neglected (often done but rarely justified), then the balance is

$$2\overline{u'_i c'}\nabla_i\bar{c} \approx -2\left(\nabla_j\bar{c}\right)K_{ji}\left(\nabla_i\bar{c}\right) \approx \overline{\dot{c}'c'}. \tag{8.18}$$

For most forms of dissipation (e.g., molecular diffusivity), $\overline{\dot{c}'c'}$ is negative definite. When $-K$ is projected into the tracer gradient on both of its indices, $-\left(\nabla_j\bar{c}\right)K_{ji}\left(\nabla_i\bar{c}\right)$, the result is negative definite for arbitrary tracer gradients if the symmetric part of K *has all positive eigenvalues*. It is not necessary for all elements of K to be positive. Relatedly, a numerical model with negative diffusivities is usually numerically unstable. However, a diffusivity tensor that has negative elements in a few coordinate systems but has positive eigenvalues is not a concern.

Attempting to infer eddy diffusivity on scales where the transport is not diffusive (e.g., $t < T_{ij}$) can be misleading (e.g., Stommel, 1949). Similarly, attempting to infer a scalar diffusivity from an anisotropic diffusive process may be misleading. A 2D example is given by rotating a diagonal K by an angle θ:

$$\begin{bmatrix} \overline{u'c'} \\ \overline{v'c'} \end{bmatrix} = -\begin{bmatrix} \kappa_{xx}\cos^2\theta + \kappa_{yy}\sin^2\theta & -\kappa_{xx}\cos\theta\sin\theta + \kappa_{yy}\cos\theta\sin\theta \\ -\kappa_{xx}\cos\theta\sin\theta + \kappa_{yy}\cos\theta\sin\theta & \kappa_{xx}\cos^2\theta + \kappa_{yy}\sin^2\theta \end{bmatrix} \begin{bmatrix} \frac{\partial \bar{c}}{\partial x} \\ \frac{\partial \bar{c}}{\partial y} \end{bmatrix} \tag{8.19}$$

If $\kappa_{xx} \gg \kappa_{yy}$ and $\frac{\partial c}{\partial x} \sim \frac{\partial c}{\partial y}$, then a diagnosis of the scalar "diffusivity" k by $\overline{u'c'} = -k\frac{\partial \bar{c}}{\partial x}$ would yield a negative "diffusivity" k for all $\pi/4 < \theta < 3\pi/4$.

2.5. Sources of Anisotropy in Oceanic Diffusion

The best-studied form of anisotropic diffusion results from diffusion in the presence of a shear flow. The resulting spreading, or shear dispersion, has a strongly anisotropic diffusion operator. In Taylor (1953, 1954), there are early quantifications of this effect, where it is demonstrated that in laminar pipe flow, the *effective diffusion* in the along-pipe direction (D_{eff}) greatly exceeds the molecular or eddy diffusion across the pipe (D). Indeed, the virtual along-pipe diffusion is inversely proportional to the small-scale (molecular) diffusion, $D_{\text{eff}}=D+U^2a^2/(48D)$, where U and a are the flow speed and pipe radius (i.e., maximum eddy scale). In oceanographic application, Okubo (1967) and Young et al. (1982) describe a related effect from oscillatory shear, such as from internal waves, interacting with small-scale turbulence. Young and Jones (1991); Jones and Young (1994) review shear dispersion work up to that date, and extend solutions toward shorter timescales and anomalous and chaotic diffusion regimes where Taylor's scaling does not apply. The jet-like structures found by Treguier et al. (2003) and Maximenko et al. (2005) or the Antarctic Circumpolar Current (Ferrari and Nikurashin, 2010) are examples of flows that should result in strong shear dispersion. Of particular relevance is Smith (2005), who develops scalings for passive tracer transport along and across quasi-geostrophic jets, and shows that the along-jet scaling is inversely proportional to the isotropic diffusivity and depends on eddy scale and flow rate much as in Taylor's theory.

Shear dispersion results from an interaction of the steady and isotropic, homogeneous eddying flows. However, other phenomena are also expected to result in anisotropic diffusion. Oceanic turbulence is quite heterogeneous, as shown in Figure 8.1. Horizontal velocities exceed vertical ones in the ocean, but it also seems likely that the two components of horizontal velocity will vary, as well as their correlations. From Equation (8.14), these effects also impact the diffusivity. Furthermore, jets and potential vorticity gradients are thought to suppress diffusivity in the cross-jet and PV-gradient direction (Rogerson et al., 1999; Ferrari and Nikurashin, 2010). Coherent structures and vortices have a strongly anisotropic direction of propagation (Griffa et al., 2008; Chelton et al., 2011). Finally, instabilities are often quite anisotropic; such "noodle" instabilities produce strong anisotropy (Berloff et al., 2009). Both "noodling" and coherent eddy drift also tend to align according to potential vorticity gradients—from the flow or from the planetary beta effect. At present it is unclear which of these effects are dominant in the ocean. Indeed, even the degree to which they are distinct from each other is presently unclear.

Two studies attempting to measure rotational effects on anisotropy found sensitive dependence on rotational fluxes (Eden and Greatbatch, 2009; Eden, 2010a). However, their method assumes a limited form for K (the symmetric part has two equal eigenvalues, which is not anisotropic diffusion in the sense described here). Furthermore, they subtract rotational contributions (Eden et al., 2007a), rendering their diagnostic framework too different from the assumptions of Taylor (1921, 1953) to compare directly. Riha and Eden (2011) find strong contrast between along- and across-front transports in agreement with other studies (Berloff et al., 2009; Ferrari and Nikurashin, 2010).

2.6. The Veronis Effect

Gravity breaks the symmetry of stratified turbulent flow, leading to anisotropic diffusion. If we assume uncorrelated velocities in each direction and reduced vertical velocities, then an anisotropic eddy diffusivity is a natural form to assume for the result of Equation (8.14):

$$K_{ij}=\begin{bmatrix}\kappa_h & 0 & 0\\ 0 & \kappa_h & 0\\ 0 & 0 & \kappa_v\end{bmatrix}_{ij} \tag{8.20}$$

This assumed diffusivity tensor is diagonal, so the eigenvalues are the diagonal elements and the eigenvectors can be taken to be the x, y, and z directions. The eigenvalues are chosen such that the diffusion in the x- and y-directions is the same, while the diffusion in the vertical direction is smaller.

Suppose that, with great effort, an oceanography cruise measures the eddy flux of temperature along a section, providing $\overline{u'\Theta'}$, $\overline{w'\Theta'}$, and $\bar{\Theta}(x,z)$. Delighted, the intrepid crew inverts to find the 2D eddy diffusivity components,

$$\overline{u_i'\Theta'}=-\begin{bmatrix}\kappa_h & 0\\ 0 & \kappa_v\end{bmatrix}_{ij}\nabla_j\bar{\Theta},\rightarrow \kappa_h(\Theta)=\frac{-\overline{u'\Theta'}}{\nabla_x\bar{\Theta}},\kappa_v(\Theta)=\frac{-\overline{w'\Theta'}}{\nabla_z\bar{\Theta}}. \tag{8.21}$$

And since the number of degrees of freedom equals the number of equations to satisfy, the result exactly satisfies the observational evidence (assuming $\nabla\bar{\Theta}\neq 0$).

The next year, another cruise measures both salinity and temperature. The temperature results prove nearly the same, aside from interannual variability, but the salinity results are confusing. The salinity fluxes are exactly predicted by diffusion formulae

$$\kappa_h(S)=\frac{-\overline{u'S'}}{\nabla_x\bar{S}},\kappa_v(S)=\frac{-\overline{w'S'}}{\nabla_z\bar{S}}, \tag{8.22}$$

but the diffusivities disagree with those diagnosed from Θ: $\kappa_h(\Theta)\neq\kappa_h(S)$, $\kappa_v(\Theta)\neq\kappa_v(S)$. How is this possible? Do salinity and temperature have different eddy diffusivities? Not necessarily.

If the salinity and temperature gradients do not align, then they will sample different combinations of diffusivity eigenvalues, and therefore be diffused differently. But, is not all that taken into account using the tensor K_{ij}? Yes, if indeed the correct form for K_{ij} was assumed in Equation (8.20), different gradient directions would be correctly treated.[6] Just as mean flows have preferred directions, so too eddy fluxes occur fastest along dynamically selected directions, which may not be horizontal and vertical. The assumed form (Equation 8.20) for K_{ij} does not allow this to occur.

Consider instead simultaneous equations on salinity and temperature,

$$\overline{u_i'\Theta'} = -R_{ij}\nabla_j\bar{\Theta},\ \overline{u_i'S'} = -R_{ij}\nabla_j\bar{S}. \tag{8.23}$$

Now for 2D observations, there are four equations, but only 2 degrees of freedom can be matched by Equation (8.20). However, a 2×2 matrix for R_{ij} will do nicely, and indeed we expect it will have a symmetric part representing diffusion with its eigenvectors aligned and perpendicular to the principal axis of maximal disturbance, regardless of whether that direction is exactly vertical or somewhat tilted.

If an incorrect form for R is used, it may still be possible to tune to reproduce the transport for one tracer as it was in Equation (8.20). However, other tracers will be diffused incorrectly. One expects largest eigenvectors to fall along the minimal-disturbance plane, so a mistaken diffusion ansatz such as Equation (8.20)—even as a numerical artifact (Griffies et al., 2000)—results in spurious diabatic or dianeutral mixing of different water masses called the *Veronis effect* (Veronis, 1975).

What if there are more than two tracers, or more than three in three dimensions? Well, since Equation (8.3) is linear in tracer concentration, the equations for tracer concentration and fluxes can be added and subtracted as desired. If all of the tracers have only a large-scale gradient, then only three whose gradients are not aligned are needed to map the diffusivity tensor and any more can be related to a linear combination of these three. However, most tracers not only have a large-scale gradient, but also variations on larger and smaller scales that differ from other tracers. In this case, a least-squares or otherwise optimized tensor can average appropriately over variations in the local gradient (Bachman and Fox-Kemper, 2013).

2.7. Streamfunction and Diffusivity

If the experiment measuring temperature and salinity fluxes were conducted in a region where small-scale mixing in the maximal-disturbance direction was weak then present theory would predict the result to be nearly (Griffies, 1998)

$$\overline{u'c'} = -\begin{bmatrix} \kappa_h & 0 \\ 2\kappa_h\mathcal{S} & \mathcal{S}\kappa_h\mathcal{S} \end{bmatrix}\nabla\bar{c}. \tag{8.24}$$

The minimal-disturbance slope appears ($\mathcal{S}$ from Section 2.1.2), and indeed the eigenvectors are aligned along it, but the tensor is not symmetric! It is perhaps easier to contemplate this as the combination of two distinct eddy effects: diffusion, the symmetric part of this tensor, and advection, represented by a streamfunction (Redi, 1982; Gent and McWilliams, 1990; Griffies, 1998; Bachman and Fox-Kemper, 2013):

$$\overline{u'c'} = -\left(\begin{bmatrix} \kappa_h & \kappa_h\mathcal{S} \\ \kappa_h\mathcal{S} & \mathcal{S}\kappa_h\mathcal{S} \end{bmatrix} + \begin{bmatrix} 0 & -\kappa_h\mathcal{S} \\ \kappa_h\mathcal{S} & 0 \end{bmatrix}\right)\nabla\bar{c}. \tag{8.25}$$

In the Taylor (1921, 1953) theory, the 3D diffusion tensor in Equation (8.14) was explicitly symmetric. This symmetry is a consequence of the fluid having constant density in that case.[7] If, instead, displaced parcels are correlated with variations in density, then an advection-like term arises. That is, if $\overline{V'\rho'} \neq 0$, then mass will tend to move in the direction the denser parcels tend to go on average, even if there is no mean velocity $\overline{V'} = 0$.

An elegant theory that helps explain this effect is that of Dukowicz and Smith (1997) (an extension of Monin and Yaglom, 1971, to compressible cases and stratified flow). In their theory, they consider stochastic relocation of fluid parcels, and the evolution of the probability distribution of the location of those parcels. The probability that a parcel originally located at $\boldsymbol{x}$ at time t will later be at z at time $t+\Delta t$ is $p(z, t+\Delta t|x, t)$. Two important quantities can be derived from this distribution, the motion of the center of the parcel displacement and the evolving correlation of displacements. These are

$$v_i(x,t) = \lim_{\Delta t\to 0}\frac{1}{\Delta t}\int d^3z(z_i - x_i)p(z,t+\Delta t|x,t), \tag{8.26}$$

$$K_{ij}(x,t) = \frac{1}{2}\lim_{\Delta t\to 0}\frac{1}{\Delta t}\int d^3z(z_i - x_i)(z_j - x_j)p(z,t+\Delta t|x,t). \tag{8.27}$$

Comparing the second relation with Equation (8.13), if the integral over all possible relocations weighted by their probability can be associated with the average used by Taylor (1921), then $(z_i - x_i) \sim X_i'$ and this K_{ij} is the equivalent to K_{ij} in Taylor's theory.

However, the centroid displacement velocity v in Equation (8.26) does not have an analog in that theory. Dukowicz and Smith (1997) show that probability-weighted

6. Although nonlocal, incomplete scale-separation effects might still be an issue.

7. Boussinesq fluids are not sufficiently constant in density to qualify, for reasons that will be made clear.

averaging over all relocations of parcels in the 3D compressible equations (Equation 8.1) yields

$$\frac{\partial \bar{\rho}}{\partial t} + \nabla_i \left(\bar{\rho} v_i - \nabla_j K_{ji} \bar{\rho} \right) = \nabla_j K_{ji} \nabla_i \bar{\rho},$$
$$\frac{\partial \overline{\rho c}}{\partial t} + \nabla_i \left(\overline{\rho c} v_i - \frac{\overline{\rho c}}{\bar{\rho}} \nabla_j K_{ji} \bar{\rho} \right) = \nabla_j K_{ji} \nabla_i \overline{\rho c} + \overline{\rho \dot{c}}. \qquad (8.28)$$

In an incompressible fluid, then the simplest way to satisfy the former is to set $\bar{u}_i = v_i - \nabla_j K_{ji}$, since incompressibility already ensures $\nabla_i \bar{u}_i = 0$.[8] This assumption relates the relocation of the probability center to the Eulerian mean velocity $\bar{u}_i$, and recovers (Equation 8.15) from the second equation above. Note that when K_{ij} varies spatially, this implies that v_i *can be divergent even in a nondivergent flow*! This property is generally true of Lagrangian velocities (Andrews and McIntyre, 1978a), and here results from the relatively few constraints placed on the stochastic parcel displacements—only the combination of diffusion and Lagrangian advection is required to conserve volume, not each independently.

If the fluid is compressible, then Equation (8.28) can still be reduced, and Dukowicz and Smith (1997) argue that the same assumption for v is the simplest. Then,

$$\frac{\partial \bar{\rho}}{\partial t} + \nabla_i [\bar{\rho} \bar{u}_i] = \nabla_j \left[K_{ji} \nabla_i \bar{\rho} \right], \quad \frac{\partial \overline{\rho c}}{\partial t} + \nabla_i \left[\overline{\rho c}\, \bar{u}_i - \frac{1}{\bar{\rho}} K_{ij} \nabla_j \bar{\rho} \right]$$
$$= \nabla_i \left(K_{ij} \nabla_j \overline{\rho c} \right) + \overline{\rho \dot{c}}. \qquad (8.29)$$

The effect of compressibility is therefore *advective* (bracketed) *and diffusive* (right side). Note that the right side is guaranteed to be diffusive, as K_{ij} is symmetric. Combining together the advective parts into U yields

$$\frac{\partial \bar{\rho}}{\partial t} + \nabla_i [\bar{\rho} U_i] = 0, \quad \frac{\partial \overline{\rho c}}{\partial t} + \nabla_i [\overline{\rho c}\, U_i]$$
$$= \nabla_i \left(K_{ij} \nabla_j \overline{\rho c} \right) + \overline{\rho \dot{c}}, \quad U_i \equiv \bar{u}_i - \frac{1}{\bar{\rho}} K_{ij} \nabla_j \bar{\rho}.$$

Dukowicz and Smith (1997) also exploit the similarity of the compressible equations (Equation 8.1) to the density-coordinate equations (Equation 8.7). Considering stochastic eddy displacements *within the ϱ surfaces* results in

$$\frac{\partial \bar{h}^{\varrho}}{\partial t} + \nabla_\alpha \left[\bar{h}^{\varrho} \left(\overline{u_\alpha}^{\varrho} - \frac{1}{\bar{h}^{\varrho}} K_{\alpha\beta} \nabla_\beta \bar{h}^{\varrho} \right) \right] = -\frac{\partial \bar{e}^{\varrho}}{\partial \varrho}, \qquad (8.30)$$

$$\frac{\partial \overline{hc}^{\varrho}}{\partial t} + \nabla_\alpha \left[\overline{hc}^{\varrho} \left(\overline{u_\alpha}^{\varrho} - \frac{1}{\bar{h}^{\varrho}} K_{\alpha\beta} \nabla_\beta \bar{h}^{\varrho} \right) \right]$$
$$= \nabla_\alpha \left[K_{\alpha\beta} \nabla_\beta \overline{hc}^{\varrho} \right] + \overline{\dot{\varrho} \dot{c}}^{\varrho} - \frac{\partial \overline{ec}^{\varrho}}{\partial \varrho} + \frac{\partial \overline{F_c}^{\varrho}}{\partial \varrho}. \qquad (8.31)$$

Here, it has been assumed that the entrainment velocity and the stochastic along-ϱ displacements are statistically independent. The form of Equations (8.30) and (8.31) can be applied directly in density-coordinate models.

The additional velocity $u_i^* = -\frac{1}{\bar{h}} K_{\alpha\beta} \nabla_\beta \bar{h}^{\varrho}$, is sometimes called the *eddy-induced velocity*, and is closely related to the quasi-Stokes and bolus velocities (McDougall and McIntosh, 2001). It is a result of the fact that as the tracer anomalies flow along the minimal layer, they may correlate with a bolus of excess water or a thinning of the layer. Just as the Stokes drift results from a correlation of larger velocities when a wave crest is present, the quasi-Stokes velocity results from a correlation between tracer anomaly and bolus presence.

The net effect of the stochastic process in Equations (8.30) and (8.31) is to move thickness h along the ϱ surfaces, horizontally and potentially anisotropically in the two horizontal directions. The eddy-induced velocity u_i^* alone is required in the thickness Equation (8.30), and both u_i^* and diffusion appear in the tracer Equation (8.31). It is incorrect to call any of the terms in Equation (8.30) a diffusion (Gent, 2011), even though the diffusivity $K_{\alpha\beta}$ appears in u_i^*.

Note that only one (four-component) diffusivity $K_{\alpha\beta}$ appears (in contrast to frequent modeling practice), which is related via Equation (8.27) to the likely correlations of displacements within the ϱ layer, just as the generalization of Taylor (1921) in Equation (8.14) relates diffusivity to the displacements of fluid parcels. These kinematic relations do not depend directly on whether c is active or passive, or if there is more than one tracer, which one is presently under consideration. Only the assumption of stochastic displacements that conserve h and ch during their displacement is required. To contrast against Eden et al. (2007a) and others who find different diffusivities for different tracers (e.g., Lee et al., 1997; Smith and Marshall, 2009), two crucial differences should be considered: (1) Was the diagnosed diffusivity sufficiently general to capture heterogeneity or anisotropy in the flow? and (2) Were the different tracers similar in their rate of non-conservative properties? Bachman and Fox-Kemper (2013) demonstrate that even when non-conservative processes are much smaller than conservative eddy transports, changing the non-conservative rates may affect the conservative rate estimates.

Transforming Equation (8.30) to depth-coordinates yields the continuity equation for the eddy-induced velocity,

$$\nabla_i \left(\bar{u}_i + u_i^* \right) = 0, \quad \nabla_i \bar{u}_i = 0 \quad \rightarrow \nabla_i u_i^* = 0. \qquad (8.32)$$

The u^* velocity as found by Dukowicz and Smith (1997) is similar, but not identical to, that utilized or diagnosed elsewhere (Andrews and McIntyre, 1978a; Plumb, 1979; Plumb and Mahlman, 1987; Gent and McWilliams, 1990; McDougall and McIntosh, 1996, 2001; Eden et al., 2007a; Eden and Greatbatch, 2009; Eden, 2010a; Bachman and Fox-Kemper, 2013). The Dukowicz and Smith (1997) velocity is distinguished by its

8. Different choices have also been explored (Dukowicz and Smith, 1997; Dukowicz and Greatbatch, 1999; Smith, 1999).

incompressibility in three dimensions and its association to the stochastic minimal-disturbance displacements of thickness and tracer. To ensure incompressibility is satisfied, often a vector streamfunction is used to generate u^*. Thus,

$$\epsilon_{ijk}\nabla_j\Psi^*_k = u^*_i. \tag{8.33}$$

For small slopes the streamfunction generates the horizontal component of the eddy-induced velocity via

$$u^*_\alpha = K_{\alpha\beta}\nabla_z\mathcal{S}_\beta = \epsilon_{\alpha jk}\nabla_j\Psi^*_k. \tag{8.34}$$

In component form,

$$u^*_x = -\nabla_z\Psi^*_y = K_{x\beta}\nabla_z\mathcal{S}_\beta,\ u^*_y = \nabla_z\Psi^*_x = K_{y\beta}\nabla_z\mathcal{S}_\beta,$$
$$u^*_z = \nabla_x\Psi^*_y - \nabla_y\Psi^*_x.$$

For arbitrary spatial variations in K, determining the streamfunction Ψ^* from u^* or K and $\mathcal{S}$ involves solving the two differential equations in z. Gent and McWilliams (1990) and Smith and Gent (2004) propose a slightly different form, which is identical if the $K_{\alpha\beta}$ are not a function of z:

$$\begin{aligned} u^{gm}_\alpha &= -\nabla_z\left(K_{\alpha\beta}\mathcal{S}_\beta\right) = \epsilon_{\alpha jk}\nabla_j\Psi^{gm}_k,\ u^{gm}_x = -\nabla_z\Psi^{gm}_y \\ &= \nabla_z\left(K_{x\beta}\mathcal{S}_\beta\right),\ u^{gm}_y = \nabla_z\Psi^{gm}_x = \nabla_z\left(K_{y\beta}\mathcal{S}_\beta\right),\ u^{gm}_z \\ &= \nabla_x\Psi^{gm}_y - \nabla_y\Psi^{gm}_x = -\nabla_\alpha\left(K_{\alpha\beta}\mathcal{S}_\beta\right). \end{aligned} \tag{8.35}$$

This form does not require solving any differential equations, except perhaps in implementing boundaries (Ferrari et al., 2010).

Another way of considering the effects of the streamfunction is as a "skew" flux of tracers along minimum-disturbance planes. To make this clear, note that the divergence of the cross-product of Ψ^* with the tracer gradient is the same as the divergence of advection of the tracer by u^*,

$$\nabla_i\left(\Psi^*_j\epsilon_{ijk}\nabla_k c\right) = \nabla_i\left(c\epsilon_{ijk}\nabla_j\Psi^*_k\right) = \nabla_i\left(cu^*_i\right). \tag{8.36}$$

The relation (8.36) depends only on the symmetry of the derivatives and the antisymmetry of ϵ, so it applies to Ψ^{gm} as well.

Ψ^{gm} has special properties if the tracer being advected is buoyancy,

$$\nabla_i\left(bu^*_i\right) = \nabla_\alpha\left(-K_{\alpha\beta}\nabla_\beta b\right) + \nabla_z\left[\left(\nabla_\alpha b\right)K_{\alpha\beta}\left(\nabla_\beta b\right)\right]. \tag{8.37}$$

Thus, the action of the Ψ^{gm} has two parts: a horizontal diffusion by the $K_{\alpha\beta}$ and the final term is an upward buoyancy transport if $K_{\alpha\beta}$ has positive eigenvalues. This vertical flux ensures consistent extraction of potential energy from the mean in Equation (8.5) by $\overline{w'b'} > 0$.

Some authors have suggested that potential vorticity conservation is more fundamental (Killworth, 1997; Dukowicz and Greatbatch, 1999; Treguier, 1999). In practice, these differences amount to relatively small corrections compared to other assumptions, if the typical displacement distance is less than a substantial range of latitude (Smith, 1999; Zhao and Vallis, 2008; Fox-Kemper and Ferrari, 2009; Grooms et al., 2011).

Griffies (1998) uses a tensor form to make the relationships above clear upon transformation to z coordinates. For an arbitrary Ψ^*, from Equation (8.34) or Equation (8.35), the divergence of tracer flux is

$$\nabla_i\overline{u'_ic'} \approx -\nabla_i\left\{\left(\begin{bmatrix} 0 & 0 & \Psi^*_y \\ 0 & 0 & -\Psi^*_x \\ -\Psi^*_y & \Psi^*_x & 0 \end{bmatrix} + \begin{bmatrix} K_{xx} & K_{xy} & K_{xz}\mathcal{S}_x \\ K_{xy} & K_{yy} & K_{yz}\mathcal{S}_z \\ K_{xz}\mathcal{S}_x & K_{yz}\mathcal{S}_z & \mathcal{S}_zK_{z\beta}\mathcal{S}_\beta \end{bmatrix}\right)_{ij}\nabla_j\bar{c}.\right\} \tag{8.38}$$

If the Gent and McWilliams (1990) form (Equation 8.35) for Ψ^{gm} is used, this simplifies to

$$\nabla_i\overline{u'_ic'} \approx -\nabla_i\left\{\begin{bmatrix} K_{xx} & K_{xy} & 0 \\ K_{xy} & K_{yy} & 0 \\ 2K_{xz}\mathcal{S}_x & 2K_{yz}\mathcal{S}_z & \mathcal{S}_zK_{z\beta}\mathcal{S}_\beta \end{bmatrix}_{ij}\nabla_j\bar{c}\right\}. \tag{8.39}$$

Now, comparing Equation (8.39) with Equations (8.24) and (8.25) connnects this theory to the hypothetical cruise data (Equation 8.24).

Eden and colleagues (Eden et al., 2007a; Eden and Greatbatch, 2008; Eden, 2010a) allow the possibility of a different eddy transport for every tracer. By doing so, they are able to simplify each tracer variance Equation (8.17), so that eddy diffusivity occurs only when non-conservative effects are present as in Equation (8.18). Their treatment is best-suited to problems where different tracers have radically different rates of variance dissipation $\overline{c'c'}$. Their diagnosis is limited in the number of degrees of freedom it can measure: expressing Equation (8.2) from both Eden et al. (2007a) and Eden et al. (2007b) in terms of R from (Equation 8.14) yields

$$\begin{aligned} \overline{u'_ib'} &= -K^{eg}_{ij}\nabla_j\bar{b} \\ &= -\begin{bmatrix} K_{\rm dia} & -B_z & B_y \\ B_z & K_{\rm dia} & -B_x \\ -B_y & B_x & K_{\rm dia} \end{bmatrix}_{ij}\nabla_j\bar{b} + \text{rotational flux}, \end{aligned} \tag{8.40}$$

which applies throughout the nearly adiabatic ocean interior. The authors are able, by choosing specialized rotational fluxes, to reduce the number of free parameters from the four here ($K_{\rm dia}$, B_x, B_y, B_z) to three that can be determined by the buoyancy flux. However, the tensor in Equation (8.38) potentially has 9 degrees of freedom, and at least 6 of them are distinct measures of turbulence statistics representing the symmetric tensor (Equation 8.14). Many of the Transformed Eulerian Mean papers propose similar diagnoses of specialized forms of R based on buoyancy fluxes alone (e.g., Andrews and McIntyre, 1976; Ferrari and Plumb, 2003). However, there are many more degrees of freedom in R than can be prescribed by the three components of a single flux, which is the root cause of the appearance of the uncertain parameters in those

analyses. It is also the reason why the diagnoses below can proceed and find reasonable diffusivities and eddy-induced advection without recourse to rotational flux manipulations.

3. OBSERVATIONS AND MODELS OF SPATIAL VARIATIONS OF EDDY STATISTICS

The isoneutral diffusivity tensor K should vary in space as the rms velocities certainly vary from location to location, as does the decorrelation timescale tensor:

$$K_{\alpha\beta} \approx \frac{1}{2}\sqrt{\overline{u'^2_\alpha}\,\overline{u'^2_\beta}}\,T_{\alpha\beta} = \frac{1}{2}\frac{\mathrm{d}D_{\alpha\beta}(\tau)}{\mathrm{d}\tau}. \qquad (8.41)$$

Further, shear dispersion effects (Taylor, 1953; Smith, 2005) and potential vorticity barrier effects (Ferrari and Nikurashin, 2010) will vary spatially as the mean flow and potential vorticity gradients vary. Measurements of the components of the K tensor are rare, even at the surface. In this section, we compare 2D measurements from surface drifters of $K_{\alpha\beta}$ with a model estimate, and then describe the variations with depth and 3D structure of the model estimate.

To begin with, consider the global distribution of horizontal eddy kinetic energy, closely related to the trace of the K tensor. Figure 8.1 shows the logarithm of the mean and eddy kinetic energy, as estimated from a high-resolution model (Grooms et al., 2011; Fox-Kemper et al., 2013), from surface drifters, and from SSALTO/DUACS multi-satellite altimetry (SSALTO/DUACS Team, 2013). Note that the products are in rough agreement, despite slightly different averaging procedures and the fact that the altimetry provides only the geostrophic velocity.[9] Eddy kinetic energy is largest surrounding the regions where the mean kinetic energy is largest, such as western boundary currents, in the tropical jets, and in the core of the Antarctic Circumpolar Current. Regions of high eddy energy are broader than the tightly concentrated mean kinetic energy, which is consistent with the formation and dispersal of eddies from instabilities of the energetic mean features and asymptotics (Grooms et al., 2011).

The mean kinetic energy is highly anisotropic, with narrow features that extend for thousands of kilometers in many cases. It seems unlikely that this structure would lead to eddies with isotropic decorrelation timescales and isotropic kinetic energy. The eddy kinetic energy is more isotropic (not shown), with typically less than a factor of 2 difference between the zonal and meridional rms velocities—much less than the ratio of the diffusion eigenvalues. These conditions suggest shear dispersion is expected to be an important source of anisotropy.

In the analysis of drifter data, it is commonly the goal to eliminate the effects of shear dispersion and measure the cross-stream diffusivity. Following Davis (1991), the first stage of calculating a diffusivity from drifter observations is correlating the displacements with the drifter velocity, after removing a time–mean velocity for each analysis location.

$$K_{\alpha\beta}(\boldsymbol{x}, t) = -\left\langle V'_\alpha(t_0|\boldsymbol{x}, t_0) X'_\beta(t_0 - t|\boldsymbol{x}, t_0)\right\rangle, \qquad (8.42)$$

where $V'_\alpha(t|\boldsymbol{x}, t_0)$ represents the value of the α component of V' at time t that passes through location $\boldsymbol{x}$ at time t_0. In practice, this quantity is calculated for lag $t - t_0$ along the trajectories of the drifters, and then averaged into spatial bins to approximate an Eulerian field of K. Comparing Equation (8.42) to Equations (8.14) and (8.27) shows the close relationship of this diffusivity estimate to the preceding ones, apart from the specific averaging operator. One of the major concerns when mapping diffusivities and time scales from drifter or float data is this use of finite bins rather than fixed positions, which makes shear dispersion magnify the resulting diffusivity (c.f., Bauer et al., 1998). In simulation experiments with isotropic eddy energy in a flow with mean shear, Oh and Zhurbas (2000) showed that shear dispersion can be minimized by eigenanalysis of the diffusivity tensor (Equation 8.41) and taking the smaller eigenvalue to represent an approximate isotropic lateral diffusivity. Smith (2005) arrives at a similar result in an idealized model. The effect of shear dispersion is then reflected almost entirely in the larger horizontal eigenvalue. Yet, in terms of parameterizations for coarse-resolution ocean models, the goal is *not* to eliminate shear dispersion, but to predict and include it correctly.

The Oh and Zhurbas (2000) approach was exploited to map diffusivities in the Pacific and Atlantic Oceans from drifter data through 1999 (Zhurbas et al., 2003; Zhurbas and Oh, 2004). The global distribution of the minor eigenvalue of K in Figure 8.2c and ratio of minor to major eigenvalue is shown in Figure 8.3, calculated from drifter data through 2010. The values were calculated using lag times of 5, 10, 15, and 20 days. The figure depicts the average of the 10, 15, and 20 day values, since these lag times exceed the integral timescale and so estimate the diffusive limit of Taylor (1921). Thus, this figure updates the results of Zhurbas and Oh (2004) and extends them into the Indian Ocean.

Anisotropic diffusion should be included in coarse-resolution model parameterizations so that the modeled general circulation matches (Equation 8.10). For this reason, both large and small drifter eigenvalues are shown

9. In the model, a mean velocity over 6 years was used as the mean, and all perturbations from that mean were taken as eddies. The figure shows two degree averages of mean KE and eddy KE. Drifter KE was calculated from drogued surface drifter trajectories. First, the trajectories were binned into trajectories originating in one degree boxes, and the mean velocity in each bin was removed. Then variability on timescales faster than 5 days was removed by lowpass filtering (Lumpkin and Garraffo, 2005; http://www.aoml.noaa.gov/phod/dac/drifter_climatology.html). The remaining variability is associated with eddy velocities u'. Horizontal MKE and EKE were then calculated for each one degree bin. The 7-day SSALTO/DUACS absolute geostrophic velocity fields were broken down into the time-mean over 1993–1999 and the perturbation KE (SSALTO/DUACS Team, 2013). Thus, all variability faster than 7 days was reduced in the averaging process as was done deliberately for the drifters. The ME and EKE from the satellites is shown on the grid of this analysis. In all datasets, the eddy kinetic energy varies by more than 2 orders of magnitude in the horizontal.

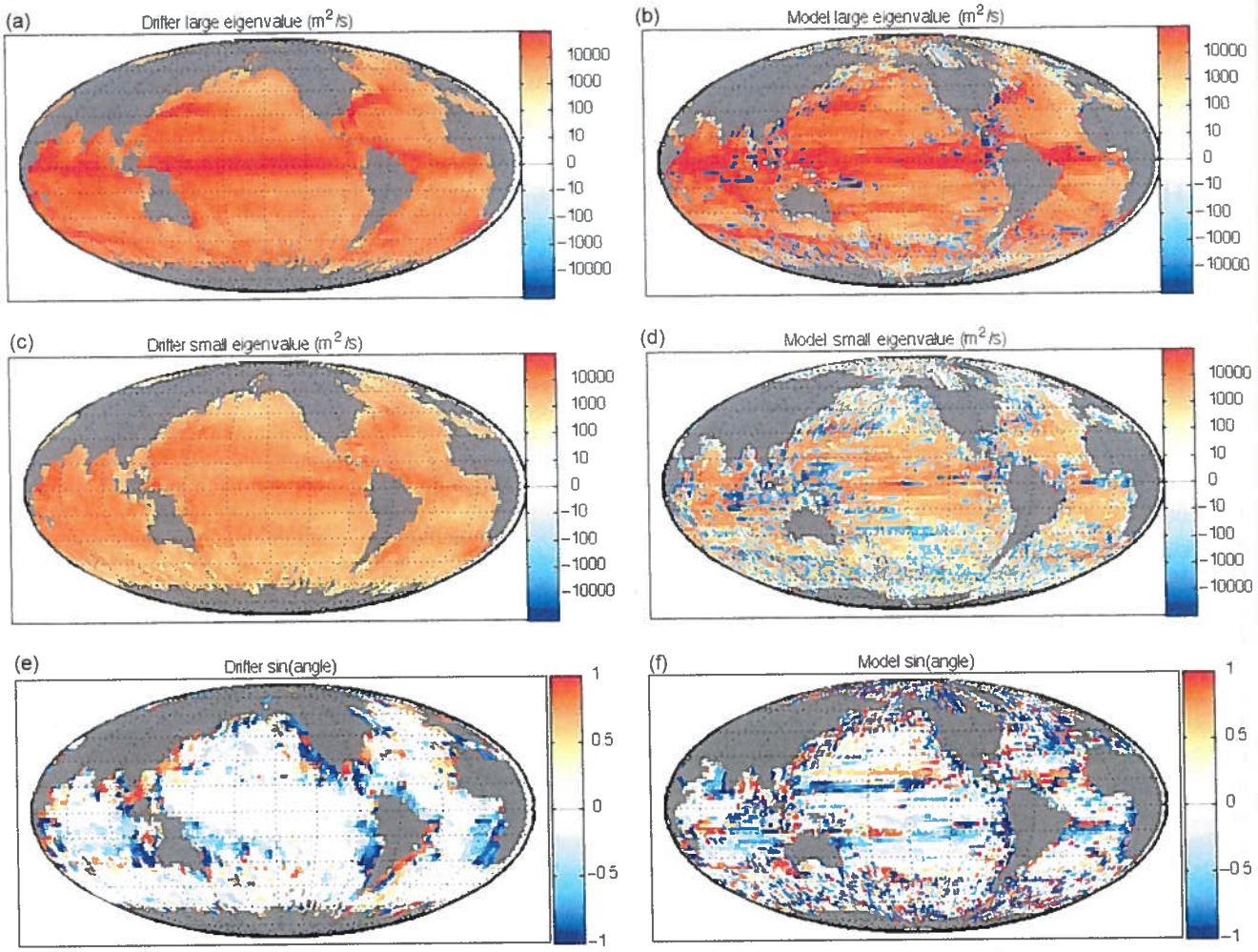

FIGURE 8.2 Surface drifter (a, c, and e) and model (b, d, and f) horizontal diffusivity eigenvalues and eigenvalue direction (sin(angle) from zonal).

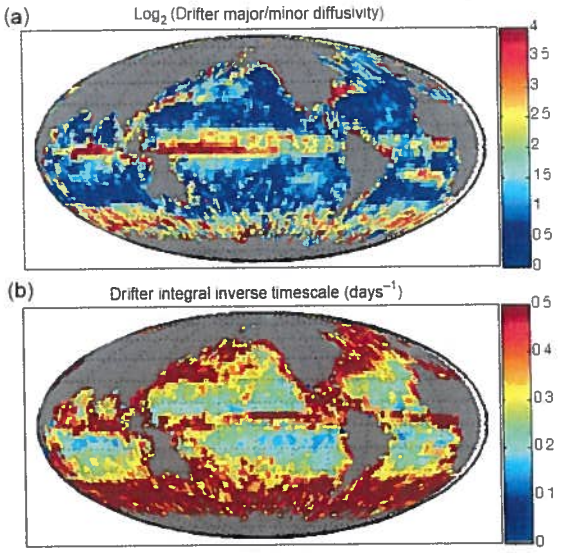

FIGURE 8.3 (a) Log of the major to minor diffusivity tensor eigenvalues from drifters. (b) Drifter integral inverse timescale (days^{-1}).

in Figure 8.2. A complementary diagnostic approach is used (Fox-Kemper et al., 2013) to produce model estimates of $K_{x\beta}$ and of the right side of Equation (8.38). Nine passive tracers (the tracers are oriented in three directions—vertical, zonal, meridional—and restored to this initial distribution with three different timescales—no restoring, 1 year restoring, and 3 year restoring) are simulated in the model already described. A least-square method (Bratseth, 1998; Bachman and Fox-Kemper, 2013) is used to invert the relationship

$$\overline{u_i' c'} = -R_{ij} \nabla_j \bar{c} + \xi, \tag{8.43}$$

and solve for the components of R and reduce the magnitude of the scatter ξ. By Equation (8.38), we expect R to be closely related to Ψ and K. The larger eigenvalues of the R tensor for the surface model gridpoint, which are associated with nearly horizontal transport, are what is shown in Figure 8.2. The inversion for R becomes indeterminate if one of the tracer gradients vanishes. Figure 8.2 shows many regions where evaluating this tensor is

compromised by the small vertical gradients in the mixed layer. However, direct comparison with the surface drifters requires the surface value (diagnosed diffusivities quickly decrease with depth). Both the minor and major eigenvalues agree between the drifters and model where the model diagnoses are not contaminated by the weak vertical tracer gradients. Despite the different methods, assumptions, models and measurement biases, and despite difficulties with exceptionally long integral timescales for the major eigenvalue, the pattern and magnitude of the eigenvalues typically agree within a factor of 2. Bachman and Fox-Kemper (2013) estimate R to within a few percent, but only in an idealized simulation.

The bottom two panels show the direction of the eigenvectors, that is, if the large horizontal eigenvalue is associated with zonal diffusion, this value is zero. While the agreement is far from perfect, away from the coastlines and boundary currents, the dominant eigenvector tends to be zonal. At the equator, this is expected from shear dispersion. It is presently unclear whether shear dispersion or additional eddy anisotropy is required to produce this effect in other regions. Figure 8.3a shows the ratio of the minor eigenvalue to major eigenvalue in the drifter data. In the regions of strong shear, such as the ACC and western boundary currents, these eigenvalues are separated by a factor of ten or more. In the gyre interior, these ratios decrease to between one and two, with the larger eigenvalue being nearly zonal.

The Lagrangian integral time and length scales are estimated by

$$T = -\frac{K_2}{\langle u_2' u_2' \rangle}, \quad L = -\frac{K_2}{\sqrt{\langle u_2' u_2' \rangle}}. \tag{8.44}$$

where K_2 is the minor horizontal eigenvalue of $K_{\alpha\beta}$ and u_2 is the minor eigenvalue of the Lagrangian velocity covariance matrix (Zhurbas et al., 2003). The global distribution of these scales is shown in Figure 8.3b. These values are qualitatively in agreement with earlier regional drifter-based studies (c.f., Krauss and Boning, 1987; Poulain and Niiler, 1989; Swenson and Niiler, 1996; Lumpkin et al., 2002). This result is consistent with Lumpkin et al. (2002), who showed that Lagrangian time scales calculated by four different methods—integrating to the first zero crossing, integrating the squared autocorrelation function to a large fixed lag (Richman et al., 1977; Lumpkin et al., 2002, use 120 days), fitting a "yardstick" to derive the integral length scale (Rupolo et al., 1996) and a parametric approach (Griffa et al., 1995)—all give qualitatively the same distribution of time scales in the North Atlantic.

The surface drifters and the model agree at the surface, but at depth the only information available is from the model. Figure 8.4 shows all components of the R tensor from the model at 318 m depth. Below the mixed layer, the tracer gradients tend not to vanish, so the model inversion is more robust. The horizontal components of the tensor (indicated by K and related to the isoneutral diffusivity) are dominantly symmetric, consistent with the Taylor (1921) and Dukowicz and Smith (1997) theory and the results of Eden (2010a). The outer row and column of R should be reduced by a factor of S, and indeed they are

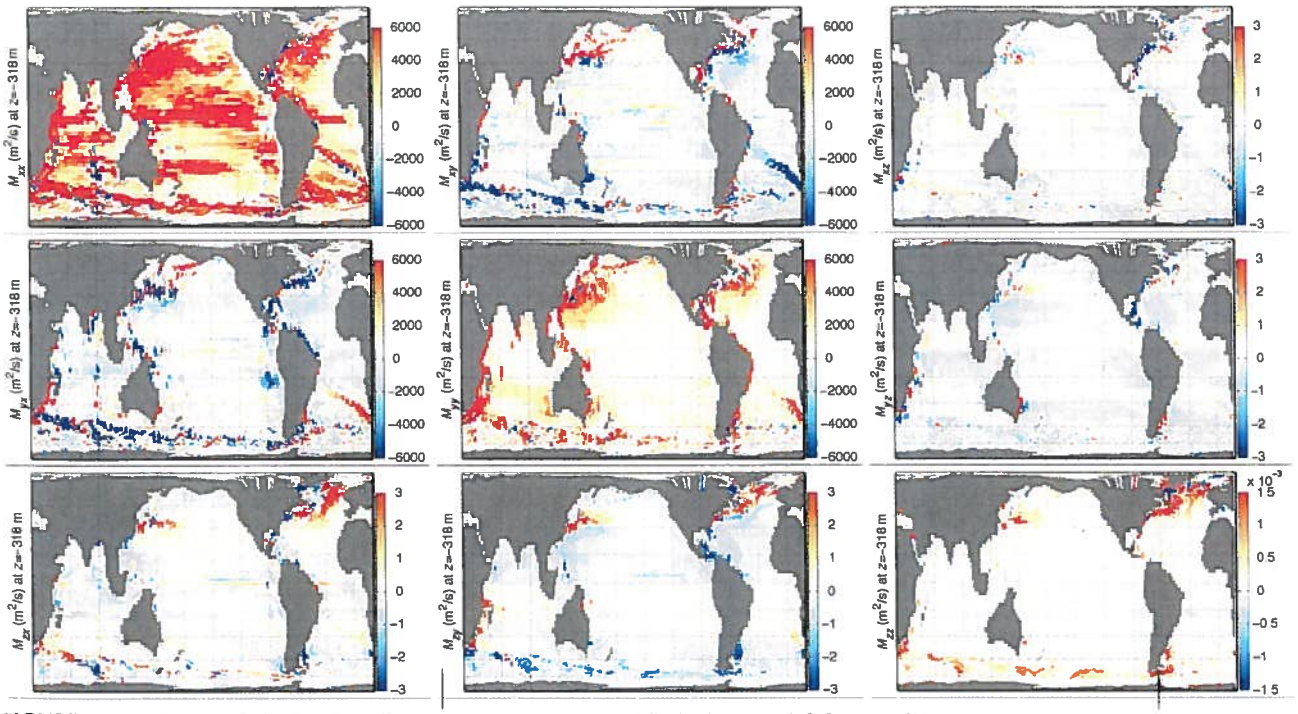

FIGURE 8.4 Components of the R tensor at 318 m depth, with the $K_{\alpha\beta}$ part in the upper left four panels.

about 1000 times smaller than the $K_{\alpha\beta}$ components. The R_{zz} component is smaller by another factor of 1000, consistent with the squared slope in Equations (8.38) and (8.39).

The outer row and column of the R tensor are not symmetric. Instead, these portions of the tensor combine the antisymmetric part related to the streamfunction and the symmetric part related to the projection of the minimal-disturbance diffusion of tracers into the vertical direction in Equation (8.38). Indeed, if the K_{ij} for these two different processes is identical and the Gent and McWilliams (1990) parameterization is correct, then as in Equation (8.39) the R_{xz} and R_{yz} elements of R should be zero. They are not exactly zero, but they are a great deal smaller than R_{zx} and R_{zy}. If the estimated uncertainty in the tracer gradient inversion above, along with uncertainty due to limited simulation length and other diagnostic issues, is taken into account, then the R_{xz} and R_{yz} elements are indistinguishable from zero in most locations (Fox-Kemper et al., 2013). Bachman and Fox-Kemper (2013) show close agreement with Equation (8.39) in an idealized model. Thus, the horizontal mixing $K_{\alpha\beta}$ that generates the symmetric and antisymmetric parts of R in the Dukowicz and Smith (1997) theory should be the same, that is, the same $K_{\alpha\beta}$ in the Gent and McWilliams (1990) parameterization as in the Redi (1982) parameterization. It is possible that small, but nonzero R_{xz} and R_{yz} elements arise from the distinction between Ψ^*, which is diagnosed in R, and Ψ^{gm} which cancels exactly in Equation (8.39). Unfortunately, the decay with depth in these fields is too weak and uncertainty too great to distinguish between Ψ^{gm} from Equation (8.35) and Ψ^* from Equation (8.34).

Figure 8.5 shows the eigenvectors and eigenvalues of the R tensor. As R is not symmetric, these eigenvalues can be imaginary, but typically they are not. Instead, the eigenvalues remain diffusion-like with positive eigenvalues, but the eigenvectors are not orthogonal (as they are for a symmetric tensor). The first eigenvalue is quite similar to the R_{xx} zonal component, and the associated eigenvectors are typically zonal. Thus, the horizontal direction of typical rapid diffusion along the neutral plane is the zonal direction. The second eigenvalue is weaker, and is often related to the R_{yy} meridional component of the R tensor. The third eigenvalue is much smaller and is related to the vertical eddy transport, the R_{zz} component of the Redi tensor. The horizontal components of the R tensor are nearly symmetric, as it should be to be consistent with the Taylor displacement correlation tensor (in agreement with the lack of such antisymmetry found by Eden, 2010a).

Fox-Kemper et al. (2013) go further in evaluating the eigenvector directions and consider their projection onto the horizontal gradient of potential vorticity. Generally, the largest direction of diffusion is perpendicular to the potential vorticity gradient, while the second largest diffusion is in the potential vorticity gradient direction, as in Ferrari and Nikurashin (2010). Where the eigenvectors are not aligned with the zonal and meridional directions is precisely where there are strong currents, consistent with both shear dispersion and transport barriers. However, it is

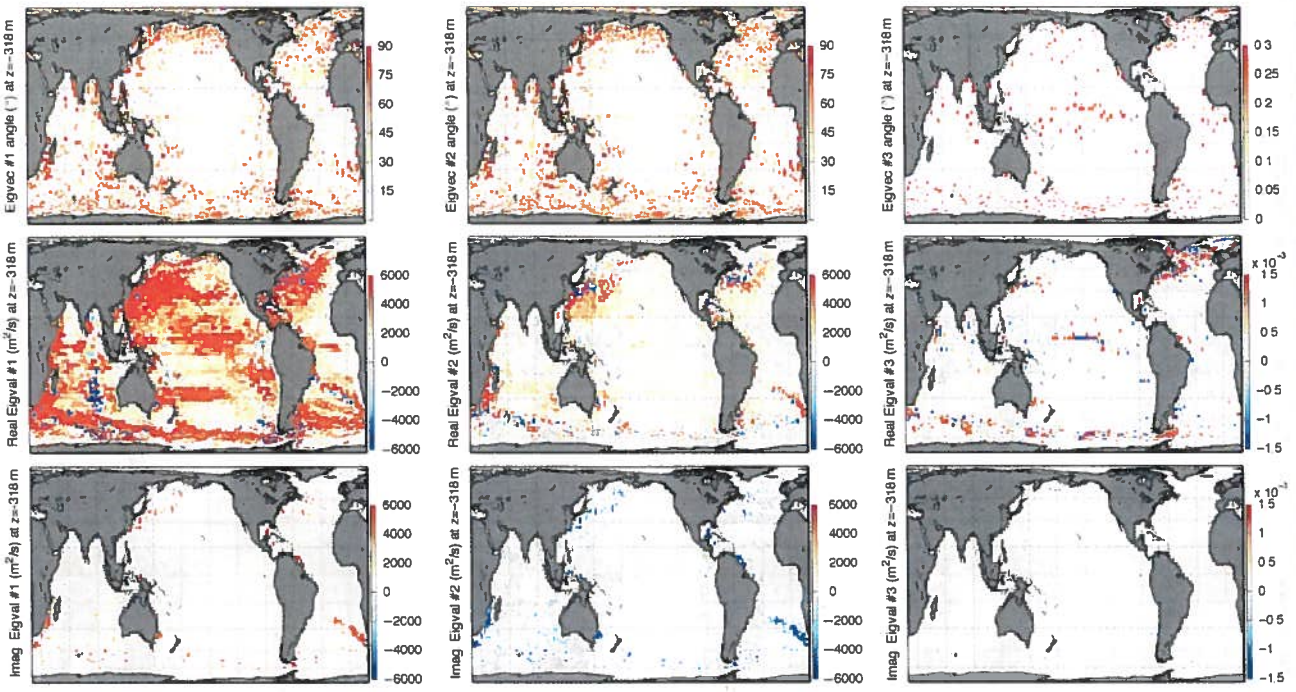

FIGURE 8.5 Eigenanalysis of the R tensor. (Top) Eigenvector direction of symmetric part of R, $(R_{ij}+R_{ji})/2$, as angle in degrees of deviation from expectation. Largest magnitude eigenvalue direction versus zonal direction (top, left), middle magnitude eigenvalue direction versus meridional direction (top, center), smallest magnitude eigenvalue direction versus vertical direction (top, right). Real (middle) and imaginary (bottom) parts of the largest eigenvalue (left), second eigenvalue (center), and smallest eigenvalue (right) of R. All values shown are at 318 m depth.

unclear if the zonal transport preference is a result of shear dispersion in zonal jets, a preference for zonal propagation of coherent eddies, or a feature of typical instabilities.

Other realistic diagnostic studies (Jayne and Marotzke, 2002; Ferreira et al., 2005; Marshall et al., 2006; Abernathey et al., 2010; Griesel et al., 2010) generally agree with the magnitude and pattern of diffusivities here. However, these studies all use a scalar diffusivity and a limited number of tracers or single tracer for diagnosis, and thus are prone to fail when the tracer gradient is not aligned with a principal diffusion axis. The Nakamura (1996) diagnosis method also reveals only a single scalar diffusivity, which is a complicated average of eigenvalues depending on contour shape. Figure 8.5 indicates that the principal axis direction is not trivially predicted, especially in the region of strong currents. Other authors have attempted to use uncertain gauge choices or other diagnostic techniques such as rotational-divergent flux decompositions to increase the ability of a scalar diffusivity to represent the data (Eden et al., 2007a; Griesel et al., 2010). However, such approaches typically rely on unmeasurable assumptions (Fox-Kemper et al., 2003). The results here indicate that the K_{ij} tensor is likely too anisotropic for such approaches to work well, in agreement with surface drifter analysis (Zhurbas and Oh, 2004).

4. MESOSCALE ISONEUTRAL DIFFUSIVITY VARIATION PARAMETERIZATIONS

Many studies have shown that the methods of parameterizing lateral transport by mesoscale and smaller features affect the general circulation (Veronis, 1975; Danabasoglu and McWilliams, 1995; Gent et al., 1995; McDougall et al., 1996; Hirst and McDougall, 1998, etc.). Increasing resolution to finer than 0.1° continues to affect the general circulation (Oschlies, 2002; Lévy et al., 2010) due to submesoscale processes (Fox-Kemper et al., 2011).

The majority of current eddy parameterization schemes are based on the work of Redi (1982) and Gent and McWilliams (1990). As described above, Griffies (1998) shows how these two important papers provide the basic flux-gradient relationship needed to represent a Dukowicz and Smith (1997) closure in a z-coordinate model. Density-coordinate models require a different form of closure Equations (8.30) and (8.31). However, all of these approaches require a prediction of the isoneutral diffusivity $K_{\alpha\beta}$, which is spatio-temporally variable and anisotropic as shown above. Cleverly, Gent and McWilliams (1990) note that this tensor needs prediction, but decline to propose how.

How to model the spatio-temporal and flow-dependent variations of $K_{\alpha\beta}$? The first conceptually successful theory specifically for this purpose is that of Visbeck et al. (1997). Their form is isotropic and based on a timescale from linear instability theory (Eady, 1949). It is

$$K_{xx} = K_{yy} = \frac{0.0015 f}{\sqrt{\mathrm{Ri}}} l_z^2 \tag{8.45}$$

where l_z is intended to be a baroclinic zone width inspired by Green (1970). However, in typical implementations, the gridscale or Rhines scale is used for l_z. Similar scalings for geophysical horizontal diffusivities based on linear instability, deformation radius, or other physical scales are also commonly discussed (Green, 1970; Stone, 1972; Larichev and Held, 1995; Held and Larichev, 1996).

Some parameterizations of the spatial variation of K are based on diagnostic analyses rather than theoretical considerations (Danabasoglu and Marshall, 2007). This approach has the advantage of getting the right pattern of diffusivity, but maybe for the wrong reasons and with the wrong sensitivity to changes in the flow.

More recently, parameterizations based on a production–dissipation of eddy kinetic energy (Eden and Greatbatch, 2008) have been tested in a simplified form (Eden et al., 2009). Under additional assumptions and simplifications, this balance can be related to a parameter similar to the Eady timescale, but one that varies with depth, so it is different from the Visbeck et al. (1997) parameterization. While this approach has the advantage over linear-instability-based approaches of being valid at finite amplitude, many aspects of the finite amplitude dynamics such as the inverse cascade, anisotropy, barotropic production, and realistic eddy kinetic energy dissipation are presently neglected. Many authors have shown that these effects contribute to the eddy fluxes of tracer (Smith et al., 2002; Arbic and Flierl, 2004; Arbic et al., 2007; Thompson and Young, 2007), so production–dissipation balances as in Eden and Greatbatch (2008) will not be fully explored until they have been extended to include such effects. Even so, Eden et al. (2009) compare the present simplified parameterizations of $K_{\alpha\beta}$, their bias from climatology data, and the level of impact on model results.

4.1. Parameterizations Versus Diagnosed K

Figure 8.6 compares the diffusivities that resulted from the different parameterizations tested by Eden et al. (2009). All of the $K_{\alpha\beta}$ they tested were horizontally isotropic, so $K_{\alpha\beta} = \kappa$, which according to Oh and Zhurbas (2000) may be compared to the smaller horizontal eigenvalue of the tensor K. While the diffusivities vary widely, the diagnosis-based (Danabasoglu and Marshall, 2007) and production–dissipation-based (Eden and Greatbatch, 2008) estimates agree with each other more than they do with any of the other estimates. Using these two parameterizations in a simulation resulted in similar modeled salinity and temperature climatologies and biases, while using a constant diffusivity and the Visbeck et al. (1997) parameterization produced radically different and less realistic simulation climatologies (Eden et al., 2009). The pattern

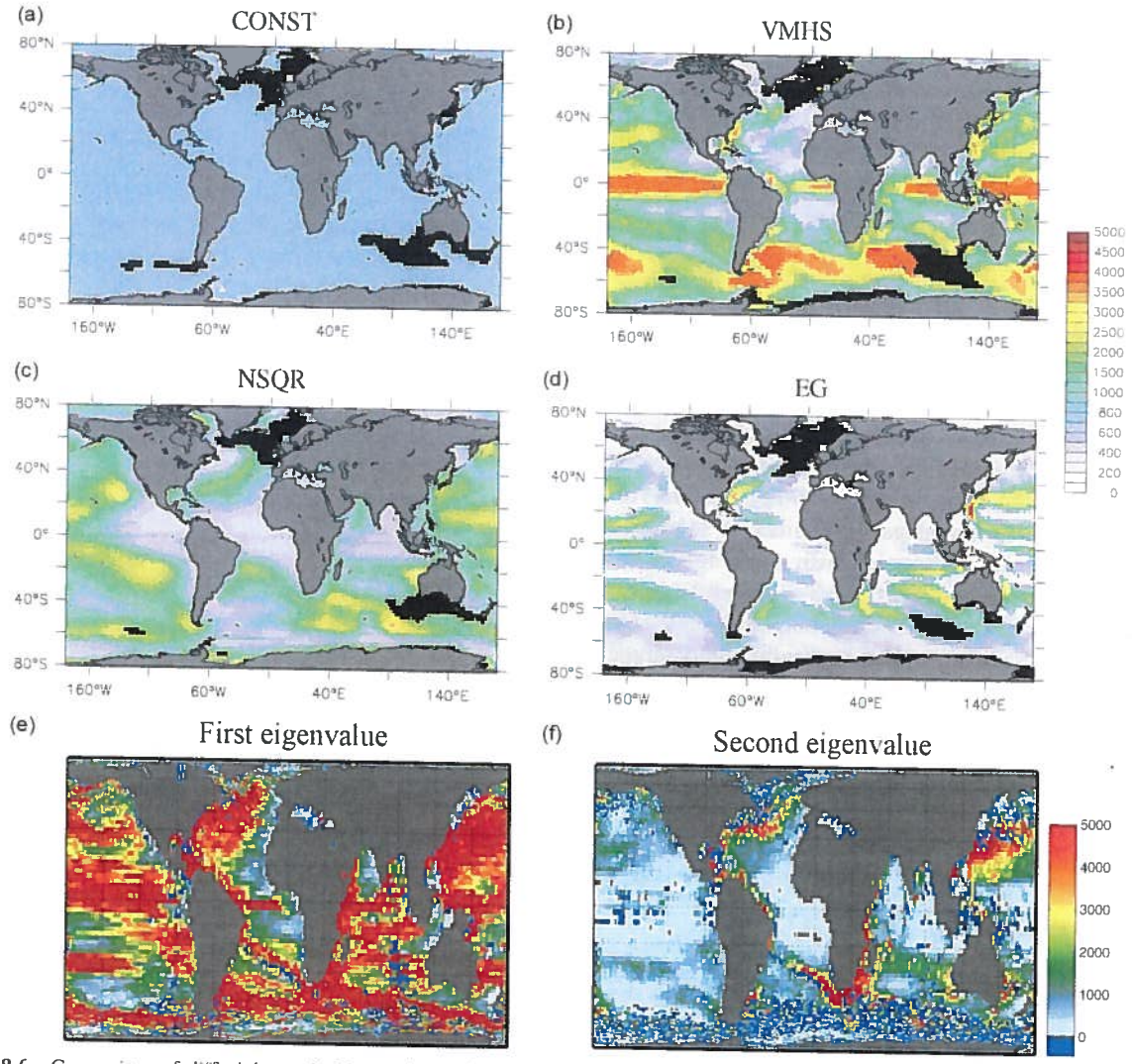

FIGURE 8.6 Comparison of diffusivity variations realized using different common parameterizations of spatial variation of (isotropic) diffusivity $K_{\alpha\beta} = \kappa$. (a) Constant diffusivity, (b) Visbeck et al. (1997), (c) Danabasoglu and Marshall (2007), (d) Eden and Greatbatch (2008), and (e and f) first and second eigenvalue from Figure 8.5. Black areas result from landmarks on the sphere remapping onto this projection. *Figures (a–d) are taken from Eden et al. (2009).*

of parameterization diffusivities (Figure 8.6c and d) is similar to the weaker horizontal eigenvalue diagnosed from the model here (Figures 8.5 (center) and 8.6f), but the parameterization magnitudes are too small. No isotropic parameterization predicts diffusivities nearly as large as the major eigenvalue in the tracer-diagnosed model (Figures 8.5 and 8.2) or drifter estimate (Figure 8.2), but a parameterization of shear dispersion might.

4.1.1. *Eddy Scales Versus Instability Scale*

Estimates of the characteristics of eddies short of prescribing a $K_{\alpha\beta}$ estimate are also useful in grounding the mixing estimates. Satellite estimates of the statistics of oceanic mesoscale variability have been invaluable in setting model parameters at realistic values and validating theory (e.g., Wunsch and Stammer, 1995; Stammer, 1997, 1998; Kushner and Held, 1998; Scott and Wang, 2005; Arbic and Scott, 2008). Other studies using data-assimilating models have been used to estimate eddy statistics (Abernathey et al., 2010; Mazloff et al., 2010; Tulloch et al., 2011). A successful parameterization will be in agreement with such estimates in terms of eddy kinetic energy (Figure 8.1), eddy integral timescale (Figure 8.3), and eddy lengthscale (related to timescale and kinetic energy). Predicting these scalars accurately allows prediction of the minor eigenvalue of $K_{\alpha\beta}$. The anisotropy of $K_{\alpha\beta}$ associated with the major eigenvalue is an additional effect, which may be associated with the longer separation distance of parcels in a sheared mean flow (Taylor, 1953), sustained eddy correlation timescales in a particular direction, or other effects.

Many argue that the integral length and timescales should be closely related to the fastest-growing or energetically favored modes from linear instability theory. Recent

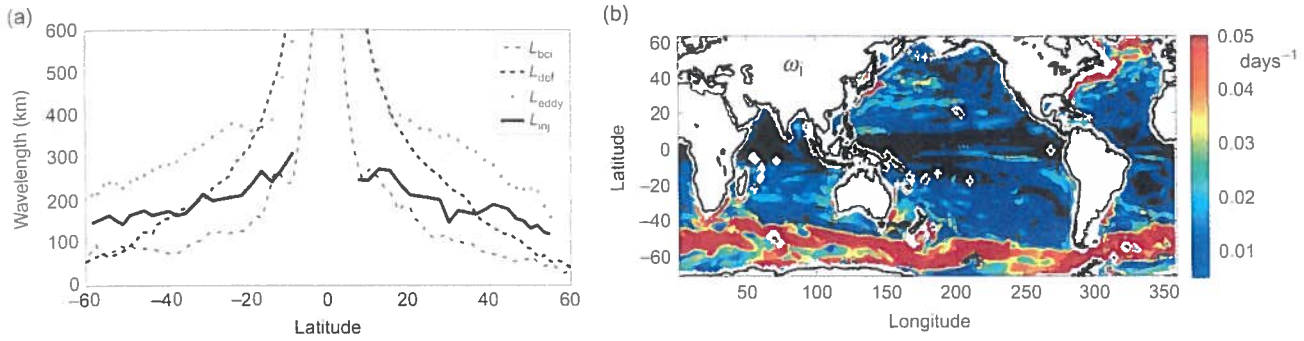

FIGURE 8.7 (a) Typical wavelength of baroclinic instability (L_{bci}), Rossby deformation radius (L_{def}), and energy-containing scale (L_{eddy}), and instability energy injection scale (L_{inj}) as estimated by Tulloch et al. (2011) based on ocean reanalysis (Forget, 2010) and AVISO altimetry. (b) Baroclinic instability inverse timescale (Tulloch et al., 2011).

studies have examined the structure, growth rates, and length scales of linear instability throughout the world, based on realistic stratification and shear profiles (Smith, 2007; Tulloch et al., 2011). The most recent and comprehensive of these studies is Tulloch et al. (2011). Figure 8.7 reproduces the most relevant results from that study—the eddy length and time scales—which may be compared to the drifter integral inverse timescale in Figure 8.3.

4.1.2. Eddy Versus Instability Spatial Scale

Even when production–dissipation balance is assumed, an additional prediction of length or time scale is needed to arrive at the units of diffusivity as in Equation (8.41). Part of the spatial-variation of K parameterization may be based on an *eddy mixing length* conceptual framework (Held and Larichev, 1996; Spall, 2000; Thompson and Young, 2007). In Eden et al. (2009) a simplified eddy lengthscale (minimum of the Rhines scale and deformation radius) is used. Prandtl (1925) first proposed a mixing length to describe momentum transfer across a boundary layer (eddy viscosity) by a mass of moving turbulent fluid. Prandtl's and Taylor's theory share a conceptual similarity to the thermodynamic mean free path. In some subgrid models, a prognostic model to predict the turbulent lengthscale is used (see Burchard and Petersen, 1999; Pope, 2000). The eddy length scale in Figure 8.7a shows that different measures of scalar eddy length scale vary by perhaps a factor of 4, which is an estimate of the magnitude of the inverse cascade. Diffusivity would be in error by the square of the error in the estimate of eddy integral lengthscale. Thus, if the (Eden et al., 2009) lengthscale were increased to reflect that the energy-containing eddy scale is 1–2 times larger than the assumed deformation radius scale, the parameterization diffusivity would be 1–4 times stronger and very close to the diagnosed K in Figure 8.6.

4.1.3. Eddy Versus Instability Time Scale

While there are some similarities in pattern, the instability timescale (Figure 8.7b) is longer than the drifter integral timescale (3b) by about a factor of 10, and the instability timescale increases as the equator is approached, consistent with $1/|f| \to \infty$. The drifter timescale is *shorter* near the equator, by contrast. Tulloch et al. (2011) argue that a particular weighting of the Eady (1949) timescale does a good job of predicting observed eddy statistics. It remains to be seen if this better linear instability timescale can improve the diffusivity in a parameterization like Visbeck et al. (1997); the disagreement between the instability and decorrelation timescales here is not encouraging.

4.2. New Parameterization Approaches and Future Developments

As is clear from the results of Eden et al. (2009), the eddy parameterization details strongly affect simulations. The Gent and McWilliams (1990) parameterization applies in the ocean interior, and treatment of how the parameterization is adjusted as a boundary is approached has recently been advanced. Early approaches used unphysical tapering schemes (Gnanadesikan et al., 2007), but recently two novel approaches have made the boundary treatment more physical. The first approach transitions from the neutral, along-ϱ surface mixing plus velocity described above to a purely horizontal diffusion in the surface layer, where diabatic effects render the approach less meaningful (Treguier et al., 1997; Danabasoglu et al., 2008; Ferrari et al., 2008). The deliberate transition from eddy transport along neutral planes to across occurs over the depth where diabatic processes occur sporadically (the transition layer) across a gridcell and is complete across the depths where diabatic processes occur consistently (the mixed layer). The second approach is that of Ferrari et al. (2010), which raises the order of Equation (8.35) to include a vertical smoothing of the streamfunction compared to the neutral slope, which they argue is related to the dominance of low-mode vertical structures in the production of the u^*. Based on the differential order of the smoothing operator, they gain extra boundary conditions that may be used to satisfy surface and bottom boundary conditions. Conceivably, a similar approach might adopt the differential form of Equation (8.34) instead of

Equation (8.35). Danabasoglu et al. (2008) and Ferrari et al. (2010) produce smoother profiles of eddy fluxes as the boundaries are approached, consistent with high-resolution models. Significantly, both novel boundary methods are independent of other specifications of the horizontal and vertical variations of $K_{\alpha\beta}$, so they may continue to be used with new parameterizations of the spatial variations.

While not a lateral transport in the ocean interior, the mixed layer eddy parameterization for submesoscale eddy restratification of Fox-Kemper et al. (2008) and Fox-Kemper et al. (2011) shares many features with the Gent and McWilliams (1990) parameterization. Bachman and Fox-Kemper (2013) show that a matching symmetric parameterization, as in Redi (1982), should be used with the Fox-Kemper et al. (2008) antisymmetric parameterization. However, the stratification and shear of the mixed layer are simpler than in the full ocean depth, so Fox-Kemper et al. (2008) were able to handle the surface and mixed layer base boundary problem conditions and the flow-dependent spatial variation of mixed layer eddies all at once. Continued development of the parameterization approaches in the previous section, guided by the diagnostic results from eddy-resolving models and data in the preceding section, may soon allow the mesoscale problem to be similarly complete.

Eddies and their transport across the Antarctic Circumpolar Current (ACC) are of present interest due to the recent DIMES experiment (Gille et al., 2007), as well as the potentially significant impact of changing winds over the ACC (Lovenduski et al., 2008). Some high-resolution models have shown that eddy sensitivity to wind may be difficult to reproduce in parameterizations (Hallberg and Gnanadesikan, 2006), but some results are more encouraging, that coarse-resolution models may be doing a reasonable job (Gent and Danabasoglu, 2011) or may be improved with new scalings (Abernathey et al., 2011). Along the way, properties of the ACC eddy transport have been discovered (Smith and Marshall, 2009; Abernathey et al., 2010; Ferrari and Nikurashin, 2010).

Currently, a number of groups are developing and using eddy-permitting models on a large or global scale (e.g., McClean et al., 2011; Delworth et al., 2012). As computer speed increases, these approaches will become standard and the coarse-resolution, eddy-free models using the mesoscale parameterizations in the preceding section will only be used in contexts such as millennial-scale and longer paleoclimate simulations, high complexity Earth system modeling, large ensemble projects, etc. This new generation of eddy-permitting models will require a different kind of parameterization, more akin to the Large Eddy Simulation subgrid models in use for engineering and boundary layer turbulence applications. Some early progress in this direction has been made (Smagorinsky, 1963; Leith, 1996; Roberts and Marshall, 1998; Griffies and Hallberg, 2000; Fox-Kemper and Menemenlis, 2008; Hecht et al., 2008; Chen et al., 2011; San et al., 2011, 2013; Graham and Ringler, 2013).

5. CONCLUSIONS AND REMAINING QUESTIONS

The processes that dominate the lateral transport in the ocean interior, both the mean flow and mesoscale eddy transport, are presently observed, diagnosed from high-resolution simulations, and parameterized in coarse resolution models with modest success. These estimates do not all agree, and many *ad hoc* assumptions are yet to be understood in a larger context of appropriate theory.

The agreement between the modeled eddy tracer transport and the anisotropic diffusivity in the surface drifter diagnosis suggests that the effects of anisotropy and shear dispersion, while perhaps not strictly part of the "eddy diffusivity," are nonetheless missing from a coarse resolution model and should be approximated with subgrid eddy closures.

It is useful to summarize here the aspects of these lateral transport processes that are clear and consistent. The transport in the ocean interior is largely along directions that minimize disturbances of energy or stratification, at a rate closely related to the mean and rms horizontal velocities and eddy correlation scales. The eddy kinetic energy, eddy length scale, and eddy time scale are not spatially homogeneous, nor are the mean flow statistics. Heterogeneity in the eddy statistics, as well as interactions with the spatially variable mean flow, lead to large variations in the rate of eddy tracer transport. There is a relationship between linear instability scales and those of the finite amplitude eddies, but distinctions between the two roughly rationalizes the disagreement in magnitude between extant parameterizations and diagnosed diffusivity eigenvalues. The horizontal eddy diffusivity is properly a tensor based on its connection to displacement covariances, and strong anisotropy is common, although continued study of mechanisms is needed to understand and properly parameterize anisotropy. Finally, observations of tracers worldwide have led to good maps of tracer concentrations against which models may be validated, but even more observations and modeling are needed to account for all tracers and correlations of interest, including the biological and chemical.

Model errors in the transport of tracers result in significant model biases, but improvement has occurred and will continue. As a general rule, parameterizations should be as simple as possible and diagnoses as general as possible. Otherwise, errors cannot be diagnosed and excessive tuning may make our solutions look good for the wrong reasons.

ACKNOWLEDGMENT

The authors thank the reviewers and editor for patient, hard work and useful suggestions that greatly improved this chapter. The altimeter products were produced by the SSALTO/DUACS Team (2013) and distributed by AVISO, with support from CNES (http://www.aviso.oceanobs.com/duacs/). B. F.-K. was supported by NSF OCE 0825614. R. L. was supported by NOAA's Office of Climate

Observations and the Atlantic Oceanographic and Meteorological Laboratory. F. O. B. was supported by NSF through its sponsorship of NCAR. The model simulations here were run by John Dennis, with resources from IBM and the NCAR CISL HPC Advisory Panel (CHAP).

REFERENCES

Abernathey, R., Marshall, J., Mazloff, M., Shuckburgh, E., 2010. Enhancement of mesoscale eddy stirring at steering levels in the southern ocean. J. Phys. Oceanogr. 40, 170–184.

Abernathey, R., Marshall, J., Ferreira, D., 2011. Dependence of Southern Ocean meridional overturning on wind stress. J. Phys. Oceanogr. 41, 2261–2278.

Andrews, D.G., McIntyre, M.E., 1976. Planetary waves in horizontal and vertical shear: asymptotic theory for equatorial waves in weak shear. J. Atmos. Sci. 33, 2049–2053.

Andrews, D.G., McIntyre, M.E., 1978a. An exact theory of nonlinear waves on a Lagrangian-mean flow. J. Fluid Mech. 89, 609–646.

Andrews, D.G., McIntyre, M.E., 1978b. Generalized Eliassen-Palm and Charney-Drazin theorems for waves on axisymmetric flows in compressible atmospheres. J. Atmos. Sci. 35, 175–185.

Arbic, B.K., Flierl, G.R., 2004. Baroclinically unstable geostrophic turbulence in the limits of strong and weak bottom Ekman friction: application to midocean eddies. J. Phys. Oceanogr. 34, 2257–2273.

Arbic, B.K., Scott, R.B., 2008. On quadratic bottom drag, geostrophic turbulence, and oceanic mesoscale eddies. J. Phys. Oceanogr. 38 (1), 84–103.

Arbic, B.K., Flierl, G.R., Scott, R.B., 2007. Cascade inequalities for forced—dissipated geostrophic turbulence. J. Phys. Oceanogr. 37, 1470–1487.

Bachman, S., Fox-Kemper, B., 2013. Eddy parameterization challenge suite. I: eady spindown. Ocean Model. 64, 12–28.

Batchelor, G.K., 1949. Diffusion in a field of homogeneous turbulence. 1. Eulerian analysis. Aust. J. Sci. Res. A Phys. Sci. 2 (4), 437–450.

Bauer, S., Swenson, M., Griffa, A., Mariano, A., Owens, K., 1998. Eddy mean flow decomposition and eddy-diffusivity estimates in the tropical Pacific Ocean 1. Methodology. J. Geophys. Res. Oceans 103 (C13), 30855–30871.

Berloff, P., 2005. On dynamically consistent eddy fluxes. Dyn. Atmos. Oceans 38, 123–146.

Berloff, P.S., McWilliams, J.C., 1999. Large-scale, low-frequency variability in wind-driven ocean gyres. J. Phys. Oceanogr. 29, 1925–1949.

Berloff, P., Kamenkovich, I., Pedlosky, J., 2009. A model of multiple zonal jets in the oceans: dynamical and kinematical analysis. J. Phys. Oceanogr. 39 (11), 2711–2734.

Bratseth, A.M., 1998. On the estimation of transport characteristics of atmospheric data sets. Tellus 50A, 451–467.

Broecker, W., 1987. The biggest chill. Nat. Hist. 96, 74–82.

Bryan, K., Dukowicz, J.K., Smith, R.D., 1999. On the mixing coefficient in the parameterization of bolus velocity. J. Phys. Oceanogr. 29 (9), 2442–2456.

Bryan, F.O., Hecht, M.W., Smith, R.D., 2007. Resolution convergence and sensitivity studies with North Atlantic circulation models. Part I: the western boundary current system. Ocean Model. 16, 141–159.

Burchard, H., Petersen, O., 1999. Models of turbulence in the marine environment—a comparative study of two-equation turbulence models. J. Mar. Syst. 21, 29–53.

Capet, X., Mcwilliams, J.C., Mokemaker, M.J., Shchepetkin, A.F., 2008. Mesoscale to submesoscale transition in the California current system. Part I: flow structure, eddy flux, and observational tests. J. Phys. Oceanogr. 38, 29–43.

Charney, J.G., 1955. The Gulf Stream as an inertial boundary layer. Proc. Natl. Acad. Sci. U.S.A. 41 (10), 731–740.

Chassignet, E.P., Garraffo, Z.D., 2001. Viscosity parameterization and the Gulf Stream separation. In: Muller, P., Henderson, D. (Eds.), From Stirring to Mixing in a Stratified Ocean. Proceedings of the 12th 'Aha Huliko'a Hawaiian Winter Workshop. University of Hawaii, pp. 37–41.

Chelton, D.B., Schlax, M.G., Samelson, R.M., 2011. Global observations of nonlinear mesoscale eddies. Prog. Oceanogr. 91 (2), 167–216.

Chen, Q., Gunzburger, M., Ringler, T., 2011. A scale-invariant formulation of the anticipated potential vorticity method. Mon. Weather Rev. 139, 2614–2629.

Danabasoglu, G., Marshall, J., 2007. Effects of vertical variations of thickness diffusivity in an ocean general circulation model. Ocean Model. 18, 122–141.

Danabasoglu, G., McWilliams, J., 1995. Sensitivity of the global ocean circulation to parameterizations of mesoscale tracer transports. J. Clim. 8 (12), 2967–2987.

Danabasoglu, G., Ferrari, R., McWilliams, J.C., 2008. Sensitivity of an ocean general circulation model to a parameterization of near-surface eddy fluxes. J. Clim. 21 (6), 1192–1208.

Davis, R., 1991. Observing the general circulation with floats. Deep Sea Res. Part A 38 (Supplement 1), S531–S557.

Delworth, T., Rosati, A., Anderson, W., Adcroft, A., Balaji, V., Benson, R., Dixon, K., Griffies, S., Lee, H., Pacanowski, R., et al., 2012. Simulated climate and climate change in the GFDL CM2. 5 High-resolution coupled climate model. J. Clim. 25, 2755–2781.

de Szoeke, R.A., Bennett, A.F., 1993. Microstructure fluxes across density surfaces. J. Phys. Oceanogr. 23 (10), 2254–2264.

Dukowicz, J., Greatbatch, R., 1999. The bolus velocity in the stochastic theory of ocean turbulent tracer transport. J. Phys. Oceanogr. 29, 2232–2239.

Dukowicz, J., Smith, R., 1997. Stochastic theory of compressible turbulent fluid transport. Phys. Fluids 9, 3523–3529.

Eady, E.T., 1949. Long waves and cyclone waves. Tellus 1, 33–52.

Eden, C., 2010a. Anisotropic rotational and isotropic residual isopycnal mesoscale eddy fluxes. J. Phys. Oceanogr. 40 (11), 2511–2524.

Eden, C., 2010b. Parameterising meso-scale eddy momentum fluxes based on potential vorticity mixing and a gauge term. Ocean Model. 32, 58–71.

Eden, C., Greatbatch, R.J., 2008. Diapycnal mixing by meso-scale eddies. Ocean Model. 23 (3–4), 113–120.

Eden, C., Greatbatch, R.J., 2009. A diagnosis of isopycnal mixing by mesoscale eddies. Ocean Model. 27 (1–2), 98–106.

Eden, C., Greatbatch, R.J., Olbers, D., 2007a. Interpreting eddy fluxes. J. Phys. Oceanogr. 37, 1282–1296.

Eden, C., Greatbatch, R.J., Willebrand, J., 2007b. A diagnosis of thickness fluxes in an eddy-resolving model. J. Phys. Oceanogr. 37, 727–742.

Eden, C., Jochum, M., Danabasoglu, G., 2009. Effects of different closures for thickness diffusivity. Ocean Model. 26 (1–2), 47–59.

Edwards, C.A., Pedlosky, J., 1998. Dynamics of nonlinear cross-equatorial flow. Part i: potential vorticity transformation. J. Phys. Oceanogr. 28 (12), 2382–2406.

Ferrari, R., Nikurashin, M., 2010. Suppression of eddy diffusivity across jets in the Southern Ocean. J. Phys. Oceanogr. 40 (7), 1501–1519.

Ferrari, R., Plumb, R.A., 2003. Residual circulation in the ocean. In: Proceedings of the 13th 'Aha Huliko'a Hawaiian Winter Workshop 13, pp. 219–228.

Ferrari, R., McWilliams, J.C., Canuto, V.M., Dubovikov, M., 2008. Parameterization of eddy fluxes near oceanic boundaries. J. Clim. 21 (12), 2770–2789.

Ferrari, R., Griffies, S.M., Nurser, A.J.G., Vallis, G.K., 2010. A boundary-value problem for the parameterized mesoscale eddy transport. Ocean Model. 32 (3–4), 143–156.

Ferreira, D., Marshall, J., Heimbach, P., 2005. Estimating eddy stresses by fitting dynamics to observations using a residual-mean ocean circulation model and its adjoint. J. Phys. Oceanogr. 35, 1891–1910.

Forget, G., 2010. Mapping ocean observations in a dynamical framework: a 2004–06 ocean atlas. J. Phys. Oceanogr. 40, 1201–1221.

Fox-Kemper, B., 2004. Wind-driven barotropic gyre II: effects of eddies and low interior viscosity. J. Mar. Res. 62 (2), 195–232.

Fox-Kemper, B., 2005. Reevaluating the roles of eddies in multiple barotropic wind-driven gyres. J. Phys. Oceanogr. 35 (7), 1263–1278.

Fox-Kemper, B., Ferrari, R., 2009. An eddifying Parsons model. J. Phys. Oceanogr. 39 (12), 3216–3227.

Fox-Kemper, B., Menemenlis, D., 2008. Can large eddy simulation techniques improve mesoscale-rich ocean models? In: Hecht, M., Hasumi, H. (Eds.), Ocean Modeling in an Eddying Regime. AGU Geophysical Monograph Series, vol. 177. Wiley, pp. 319–338.

Fox-Kemper, B., Pedlosky, J., 2004. Wind-driven barotropic gyre I: circulation control by eddy vorticity fluxes to an enhanced removal region. J. Mar. Res. 62 (2), 169–193.

Fox-Kemper, B., Ferrari, R., Pedlosky, J., 2003. On the indeterminacy of rotational and divergent eddy fluxes. J. Phys. Oceanogr. 33 (2), 478–483.

Fox-Kemper, B., Ferrari, R., Hallberg, R., 2008. Parameterization of mixed layer eddies. Part I: theory and diagnosis. J. Phys. Oceanogr. 38 (6), 1145–1165.

Fox-Kemper, B., Danabasoglu, G., Ferrari, R., Griffies, S.M., Hallberg, R.W., Holland, M.M., Maltrud, M.E., Peacock, S., Samuels, B.L., 2011. Parameterization of mixed layer eddies. III: implementation and impact in global ocean climate simulations. Ocean Model. 39, 61–78.

Fox-Kemper, B., Bryan, F.O., Dennis, J., 2013. Global diagnosis of the mesoscale eddy flux tracer gradient relationship. Ocean Model. in preparation.

Fratantoni, D.M., 2001. North atlantic surface circulation during the 1990's observed with satellite-tracked drifters. J. Geophys. Res. 106 (C10), 22,067–22,093.

Frenkiel, F.N., 1952. On the statistical theory of turbulent diffusion. Proc. Natl. Acad. Sci. U.S.A. 38 (6), 509–515.

Gent, P.R., 2011. The Gent–Mcwilliams parameterization: 20/20 hindsight. Ocean Model. 39, 2–9.

Gent, P.R., Danabasoglu, G., 2011. Response to increasing Southern Hemisphere winds in CCSM4. J. Clim. 24, 4992–4998.

Gent, P.R., McWilliams, J.C., 1990. Isopycnal mixing in ocean circulation models. J. Phys. Oceanogr. 20, 150–155.

Gent, P.R., McWilliams, J.C., 1996. Eliassen-palm fluxes and the momentum equation in non-eddy-resolving ocean circulation models. J. Phys. Oceanogr. 26, 2539–2546.

Gent, P.R., Willebrand, J., McDougall, T.J., McWilliams, J.C., 1995. Parameterizing eddy-induced tracer transports in ocean circulation models. J. Phys. Oceanogr. 25, 463–474.

Gille, S.T., Speer, K., Ledwell, J.R., Naveira Garabato, A.C., 2007. Mixing and stirring in the Southern Ocean. Eos 88, 39.

Gnanadesikan, A., Griffies, S.M., Samuels, B.L., 2007. Effects in a climate model of slope tapering in neutral physics schemes. Ocean Model. 16 (1–2), 1–16.

Gordon, A.L., Weiss, R., Smethie Jr., W., Warner, M., 1992. Thermocline and intermediate water communication. J. Geophys. Res. 97 (C5), 7223–7240.

Graham, J.P., Ringler, T., 2013. A framework for the evaluation of turbulence closures used in mesoscale ocean large-eddy simulations. Ocean Model. 65, 25–39.

Greatbatch, R.J., Lamb, K.G., 1990. On parameterizing vertical mixing of momentum in non-eddy-resolving ocean models. J. Phys. Oceanogr. 20, 1634–1637.

Greatbatch, R.J., McDougall, T.J., 2003. The non-Boussinesq temporal residual mean. J. Phys. Oceanogr. 33 (6), 1231–1239.

Green, J.S.A., 1970. Transfer properties of the large-scale eddies and the general circulation of the atmosphere. Q. J. R. Meteorol. Soc. 96, 157–185.

Griesel, A., Gille, S.T., Sprintall, J., McClean, J.L., LaCasce, J.H., Maltrud, M.E., 2010. Isopycnal diffusivities in the Antarctic Circumpolar Current inferred from Lagrangian floats in an eddying model. J. Geophys. Res. Oceans 115, C06006.

Griffa, A., Owens, K., Piterbarg, L., Rozovskii, B., 1995. Estimates of turbulence parameters from Lagrangian data using a stochastic particle model. J. Mar. Res. 53 (3), 371–401.

Griffa, A., Lumpkin, R., Veneziani, M., 2008. Cyclonic and anticyclonic motion in the upper ocean. Geophys. Res. Lett. 35 (1), L01608.

Griffies, S.M., 1998. The Gent-McWilliams skew flux. J. Phys. Oceanogr. 28 (5), 831–841.

Griffies, S.M., 2004. Fundamentals of Ocean Climate Models. Princeton University Press, Princeton, NJ.

Griffies, S.M., Adcroft, A.J., 2008. Formulating the equations for ocean models. In: Hecht, M., Hasumi, H. (Eds.), Ocean Modeling in an Eddying Regime. AGU Geophysical Monograph Series, vol. 177. Wiley, pp. 281–317.

Griffies, S., Hallberg, R., 2000. Biharmonic friction with a smagorinsky-like viscosity for use in large-scale eddy-permitting ocean models. Mon. Weather Rev. 128 (8), 2935–2946.

Griffies, S., Pacanowski, R., Hallberg, R., 2000. Spurious diapycnal mixing associated with advection in a z-coordinate ocean model. Mon. Weather Rev. 128 (3), 538–564.

Grooms, I., Julien, K., Fox-Kemper, B., 2011. On the interactions between planetary geostrophy and mesoscale eddies. Dyn. Atmos. Oceans 51, 109–136.

Hallberg, R., 2000. Time integration of diapycnal diffusion and richardson number-dependent mixing in isopycnal coordinate ocean models. Mon. Weather Rev. 128 (5), 1402–1419.

Hallberg, R., Gnanadesikan, A., 2006. The role of eddies in determining the structure and response of the wind-driven southern hemisphere overturning: results from the Modeling Eddies in the Southern Ocean (MESO) project. J. Phys. Oceanogr. 36 (12), 2232–2252.

Haynes, P., McIntyre, M.E., 1987. On the evolution of vorticity and potential vorticity in the presence of diabatic heating and frictional or other forces. J. Atmos. Sci. 44, 828–841.

Hecht, M.W., Holm, D.D., Petersen, M.R., Wingate, B.A., 2008. Implementation of the LANS-alpha turbulence model in a primitive equation ocean model. J. Comput. Phys. 227 (11), 5691–5716.

Held, I.M., Larichev, V.D., 1996. A scaling theory for horizontally homogeneous baroclinically unstable flow on a beta plane. J. Atmos. Sci. 53, 946–952.

Henning, C.C., Vallis, G.K., 2004. The effects of mesoscale eddies on the main subtropical thermocline. J. Phys. Oceanogr. 34 (11), 2428–2443.

Henning, C.C., Vallis, G.K., 2005. The effects of mesoscale eddies on the stratification and transport of an ocean with a circumpolar channel. J. Phys. Oceanogr. 35 (5), 880–896.

Hirst, A., McDougall, T., 1998. Meridional overturning and dianeutral transport in a z-coordinate ocean model including eddy-induced advection. J. Phys. Oceanogr. 28 (6), 1205–1223.

Holland, W.R., Lin, L.B., 1975. On the origin of mesoscale eddies and their contribution to the general circulation of the ocean. I. A preliminary numerical experiment. J. Phys. Oceanogr. 5, 642–657.

Holland, W.R., Rhines, P.B., 1980. An example of eddy-induced ocean circulation. J. Phys. Oceanogr. 10, 1010–1031.

Hoskins, B.J., McIntyre, M.E., Robertson, A.W., 1985. On the use and significance of isentropic potential vorticity maps. Q. J. R. Meteorol. Soc. 111 (470).

Jayne, S., Marotzke, J., 2002. The oceanic eddy heat transport. J. Phys. Oceanogr. 32 (12), 3328–3345.

Jochum, M., Malanotte-Rizzoli, P., 2003. On the generation of North Brazil Current rings. J. Mar. Res. 61 (2), 147–173.

Jochum, M., Danabasoglu, G., Holland, M., Kwon, Y.O., Large, W.G., 2008. Ocean viscosity and climate. J. Geophys. Res. Oceans 113 (C6).

Johnson, G.C., Bryden, H.L., 1989. On the size of the Antarctic Circumpolar Current. Deep Sea Res. Part A 36 (1), 39–53.

Jones, S.W., Young, W.R., 1994. Shear dispersion and anomalous diffusion by chaotic advection. J. Fluid Mech. 280, 149–172.

Killworth, P.D., 1997. On the parameterization of eddy transfer. Part I: theory. J. Mar. Res. 55, 1171–1197.

Krauss, W., Boning, C.W., 1987. Lagrangian properties of eddy fields in the northern North Atlantic as deduced from satellite-tracked buoys. J. Mar. Res. 45 (259–291).

Kravtsov, S., Berloff, P., Dewar, W.K., Ghil, M., McWilliams, J.C., 2006. Dynamical origin of low-frequency variability in a highly nonlinear midlatitude coupled model. J. Clim. 19, 6391–6408.

Kushner, P.J., Held, I.M., 1998. A test, using atmospheric data, of a method for estimating oceanic eddy diffusivity. Geophys. Res. Lett. 25, 4213–4216.

Large, W.G., Yeager, S.G., 2004. Diurnal to decadal global forcing for ocean and sea-ice models: the data sets and flux climatologies. NCAR Technical Note. NCAR/TN-460+STR.

Larichev, V.D., Held, I.M., 1995. Eddy amplitudes and fluxes in a homogeneous model of fully developed baroclinic instability. J. Phys. Oceanogr. 25, 2285–2297.

Lee, M.-M., Marshall, D.P., Williams, R.G., 1997. On the eddy transfer of tracers: advective or diffusive? J. Mar. Res. 55, 483–505.

Leith, C.E., 1996. Stochastic models of chaotic systems. Phys. D 98, 481–491.

Levitus, S., Conkright, M.E., Reid, J.L., Najjar, R.G., Mantyla, A., 1993. Distribution of nitrate, phosphate and silicate in the world oceans. Prog. Oceanogr. 31 (3), 245–273.

Lévy, M., Klein, P., Tréguier, A.-M., Iovino, D., Madec, G., Masson, S., Takahashi, K., 2010. Modifications of gyre circulation by sub-mesoscale physics. Ocean Model. 34, 1–15.

Lovenduski, N.S., Gruber, N., Doney, S.C., 2008. Toward a mechanistic understanding of the decadal trends in the Southern Ocean carbon sink. Global Biogeochem. Cycles 22 (3).

Lozier, M.S., 1997. Evidence for large-scale eddy-driven gyres in the North Atlantic. Science 277 (5324), 361–364.

Lozier, M.S., 2010. Deconstructing the conveyor belt. Science 328 (5985), 1507–1511.

Lumpkin, R., Elipot, S., 2010. Surface drifter pair spreading in the North Atlantic. J. Geophys. Res. Oceans 115, C12017.

Lumpkin, R., Garraffo, Z., 2005. Evaluating the decomposition of tropical Atlantic drifter observations. J. Atmos. Oceanic. Technol. 22 (9), 1403–1415.

Lumpkin, R., Garzoli, S.L., 2005. Near-surface circulation in the tropical Atlantic Ocean. Deep Sea Res. Part I 52 (3), 495–518.

Lumpkin, R., Treguier, A., Speer, K., 2002. Lagrangian eddy scales in the northern Atlantic Ocean. J. Phys. Oceanogr. 32, 2425–2440.

Luyten, J.R., Pedlosky, J., Stommel, H., 1983. The ventilated thermocline. J. Phys. Oceanogr. 13, 292–309.

Mahadevan, A., 2006. Modeling vertical motion at ocean fronts: are non-hydrostatic effects relevant at submesoscales? Ocean Model. 14, 222–240.

Maltrud, M.E., McClean, J.L., 2005. An eddy resolving global 1/10° ocean simulation. Ocean Model. 8, 31–54.

Marshall, J.C., Shutts, G., 1981. A note on rotational and divergent eddy fluxes. J. Phys. Oceanogr. 11, 1677–1680.

Marshall, J., Shuckburgh, E., Jones, H., Hill, C., 2006. Estimates and implications of surface eddy diffusivity in the Southern Ocean derived from tracer transport. J. Phys. Oceanogr. 36 (9), 1806–1821.

Marshall, D.P., Maddison, J.R., Berloff, P.S., 2012. A framework for parameterizing eddy potential vorticity fluxes. J. Phys. Oceanogr. 42, 539–557.

Maximenko, N.A., Bang, B., Sasaki, H., 2005. Observational evidence of alternating zonal jets in the world ocean. Geophys. Res. Lett. 32 (L12607). http://dx.doi.org/10.1029/2005GL022728.

Mazloff, M.R., Heimbach, P., Wunsch, C., 2010. An eddy-permitting Southern Ocean state estimate. J. Phys. Oceanogr. 40 (5), 880–899.

McClean, J.L., Maltrud, M.E., Bryan, F.O., 2006. Measures of the fidelity of eddying ocean models. Oceanography 19, 104–117.

McClean, J.L., Bader, D.C., Bryan, F.O., Maltrud, M.E., Dennis, J.M., Mirin, A.A., Jones, P.W., Kim, Y.Y., Ivanova, D.P., Vertenstein, M., Boyle, J.S., Jacob, R.L., Norton, N., Craig, A., Worley, P.H., 2011. A prototype two-decade fully-coupled fine-resolution CCSM simulation. Ocean Model. 39, 10–30.

McDougall, T.J., 1987. Neutral surfaces. J. Phys. Oceanogr. 17, 1950–1964.

McDougall, T., 2003. Potential enthalpy: a conservative oceanic variable for evaluating heat content and heat fluxes. J. Phys. Oceanogr. 33 (5), 945–963.

McDougall, T., Dewar, W., 1998. Vertical mixing and cabbeling in layered models. J. Phys. Oceanogr. 28 (7), 1458–1480.

McDougall, T.J., Jackett, D.R., 2007. The thinness of the ocean in s-theta-p space and the implications for mean diapycnal advection. J. Phys. Oceanogr. 37, 1714–1732.

McDougall, T.J., Klocker, A., 2010. An approximate geostrophic streamfunction for use in density surfaces. Ocean Model. 32 (3–4), 105–117.

McDougall, T.J., McIntosh, P.C., 1996. The temporal-residual mean velocity. Part I: derivation and the scalar conservation equations. J. Phys. Oceanogr. 26, 2653–2665.

McDougall, T.J., McIntosh, P.C., 2001. The temporal-residual-mean velocity. Part II: isopycnal interpretation and the tracer and momentum equations. J. Phys. Oceanogr. 31, 1222–1246.

McDougall, T., Hirst, A., England, M., McIntosh, P., 1996. Implications of a new eddy parameterization for ocean models. Geophys. Res. Lett. 23 (16), 2085–2088.

McDougall, T., Greatbatch, R., Lu, Y., 2002. On conservation equations in oceanography: how accurate are boussinesq ocean models? J. Phys. Oceanogr. 32 (5), 1574–1584.

McWilliams, J.C., Flierl, G.R., 1976. Optimal, quasi-geostrophic wave analyses of mode array data. Deep Sea Res. 23, 285–300.

Monin, A.S., Yaglom, A.M., 1971. Statistical Fluid Mechanics: Mechanics of Turbulence. MIT Press, Cambridge, MA, English, updated Edition.

Monin, A.S., Yaglom, A.M., Lumley, J.L., 2007. Statistical Fluid Mechanics: Mechanics of Turbulence. Dover Publications, Mineola, NY.

Munk, W.H., 1950. On the wind-driven ocean circulation. J. Meteorol. 7 (2), 79–93.

Nakamura, N., 1996. Two-dimensional mixing, edge formation, and permeability diagnosed in an area coordinate. J. Atmos. Sci. 53, 1524–1537.

Nurser, A., 1988. The distortion of a baroclinic Fofonoff gyre by wind forcing. J. Phys. Oceanogr. 18, 243–257.

Nycander, J., 2011. Energy conversion, mixing energy, and neutral surfaces with a nonlinear equation of state. J. Phys. Oceanogr. 41 (1), 28–41.

Oh, I., Zhurbas, V., 2000. Study of spatial spectra of horizontal turbulence in the ocean using drifter data. J. Phys. Oceanogr. 30 (7), 1790–1801.

Okubo, A., 1967. Effect of shear in an oscillatory current on horizontal diffusion from an instantaneous source. Int. J. Oceanol. Limnol. 1 (3), 194–204.

Oschlies, A., 2002. Improved representation of upper-ocean dynamics and mixed layer depths in a model of the North Atlantic on switching from eddy-permitting to eddy-resolving grid resolution. J. Phys. Oceanogr. 32, 2277–2298.

Parsons, A.T., 1969. A two-layer model of Gulf Stream separation. J. Fluid Mech. 39, 511–528.

Pedlosky, J., 1984. The equations for geostrophic motion in the ocean. J. Phys. Oceanogr. 14 (2), 448–455.

Plumb, R.A., 1979. Eddy fluxes of conserved quantities by small-amplitude waves. J. Atmos. Sci. 36, 1699–1704.

Plumb, R.A., Mahlman, J.D., 1987. The zonally averaged transport characteristics of the GFDL general circulation/transport model. J. Atmos. Sci. 44, 298–327.

Pope, S.B., 2000. Turbulent Flows. Cambridge University Press, Cambridge.

Poulain, P.M., Niiler, P.P., 1989. Statistical analysis of the surface circulation in the California Current System using satellite-tracked drifters. J. Phys. Oceanogr. 19, 1588–1603.

Prandtl, L., 1925. Bericht uber die entstehung der turbulenz. Z. Angew. Math. Mech. 5, 136–139.

Radko, T., Marshall, J., 2004. The leaky thermocline. J. Phys. Oceanogr. 34, 1648–1662.

Radko, T., Marshall, J., 2006. The Antarctic Circumpolar Current in three dimensions. J. Phys. Oceanogr. 36, 651–669.

Redi, M.H., 1982. Oceanic isopycnal mixing by coordinate rotation. J. Phys. Oceanogr. 12, 1154–1158.

Rhines, P.B., 1986. Vorticity dynamics of the oceanic general circulation. Annu. Rev. Fluid Mech. 18, 433–497.

Rhines, P.B., Holland, W.R., 1979. A theoretical discussion of eddy-driven mean flows. Dyn. Atmos. Oceans 3, 289–325.

Rhines, P.B., Young, W.R., 1982. Homogenization of potential vorticity in planetary gyres. J. Fluid Mech. 122, 347–367.

Richman, J., Wunsch, C., Hogg, N., 1977. Space and time scales of mesoscale motion in the western North Atlantic. Rev. Geophys. Space Phys. 15, 385–420.

Riha, S., Eden, C., 2011. Lagrangian and Eulerian lateral diffusivities in zonal jets. Ocean Model. 39 (1–2), 114–124.

Roberts, M.J., Marshall, D.P., 1998. Do we require adiabatic dissipation schemes in eddy-resolving models? J. Phys. Oceanogr. 28, 2050–2063.

Rogerson, A.M., Miller, P.D., Pratt, L.J., Jones, C.K.R.T., 1999. Lagrangian motion and fluid exchange in a barotropic meandering jet. J. Phys. Oceanogr. 29, 2635–2655.

Rupolo, V., Hua, B.L., Provenzale, A., Artale, V., 1996. Lagrangian velocity spectra at 700 m in the western North Atlantic. J. Phys. Oceanogr. 26, 1591–1607.

Samelson, R.M., Vallis, G.K., 1997. Large-scale circulation with small diapycnal diffusion: the two thermocline limit. J. Mar. Res. 55, 223–275.

San, O., Staples, A.E., Wang, Z., Iliescu, T., 2011. Approximate deconvolution large eddy simulation of a barotropic ocean circulation model. Ocean Model. 40, 120–132.

San, O., Staples, A.E., Iliescu, T., 2013. Approximate deconvolution large eddy simulation of a stratified two-layer quasigeostrophic ocean model. Ocean Model. 63, 1–20.

Scott, R.B., Straub, D.N., 1998. Small viscosity behavior of a homogeneous, quasigeostrophic, ocean circulation model. J. Mar. Res. 56, 1225–1258.

Scott, R.B., Wang, F., 2005. Direct evidence of an oceanic inverse kinetic energy cascade from satellite altimetry. J. Phys. Oceanogr. 35, 1650–1666.

Sheremet, V.A., 2004. Laboratory experiments with tilted convective plumes on a centrifuge: a finite angle between the buoyancy force and the axis of rotation. J. Fluid Mech. 506, 217–244.

Smagorinsky, J., 1963. General circulation experiments with the primitive equations I: the basic experiment. Mon. Weather Rev. 91 (3), 99–164.

Smith, R.D., 1999. The primitive equations in the stochastic theory of adiabatic stratified turbulence. J. Phys. Oceanogr. 29, 1865–1880.

Smith, K., 2005. Tracer transport along and across coherent jets in two-dimensional turbulent flow. J. Fluid Mech. 544, 133–142.

Smith, K.S., 2007. The geography of linear baroclinic instability in earth's oceans. J. Mar. Res. 65 (5), 655–683.

Smith, R., Gent, P., 2004. Anisotropic Gent-McWilliams parameterization for ocean models. J. Phys. Oceanogr. 34, 2541–2564.

Smith, K.S., Marshall, J., 2009. Evidence for enhanced eddy mixing at middepth in the Southern Ocean. J. Phys. Oceanogr. 39 (1), 50–69.

Smith, R., McWilliams, J., 2003. Anisotropic horizontal viscosity for ocean models. Ocean Model. 5, 129–156.

Smith, K.S., Boccaletti, G., Henning, C.C., Marinov, I., Tam, C.Y., Held, I.M., Vallis, G.K., 2002. Turbulent diffusion in the geostrophic inverse cascade. J. Fluid Mech. 469, 13–48.

Spall, M.A., 2000. Generation of strong mesoscale eddies by weak ocean gyres. J. Mar. Res. 58 (1), 97–116.

SSALTO/DUACS Team, 2013. SSALTO/DUACS user handbook: (M) SLA and (M)ADT near-real time and delayed time products. Tech. Rep. CLS-DOS-NT-06-034, SALP-MU-P-EA-21065-CLS, Centre National d'Etudes Spatiales.

Stammer, D., 1997. Global characteristics of ocean variability estimated from regional TOPEX/Poseidon altimeter measurements. J. Phys. Oceanogr. 27, 1743–1769.

Stammer, D., 1998. On eddy characteristics, eddy transports, and mean flow properties. J. Phys. Oceanogr. 28, 727–739.

Stommel, H.M., 1949. Horizontal diffusion due to oceanic turbulence. J. Mar. Res. 8, 199–225.

Stommel, H., Arons, A.B., 1960. On the abyssal circulation of the world ocean—II. An idealized model of the circulation pattern and amplitude in oceanic basins. Deep Sea Res. 6, 217–233.

Stommel, H., Schott, F., 1977. Beta spiral and determination of absolute velocity-field from hydrographic station data. Deep Sea Res. 24, 325–329.

Stone, P.H., 1972. A simplified radiative-dynamical model for the static stability of rotating atmospheres. J. Atmos. Sci. 29 (3).

Sverdrup, H.U., 1947. Wind-driven currents in a baroclinic ocean; with appplication to the equatorial currents of the eastern Pacific. Proc. Natl. Acad. Sci. U.S.A. 33, 318–326.

Swenson, M.S., Niiler, P.P., 1996. Statistical analysis of the surface circulation. J. Geophys. Res. Oceans 101 (C10), 22631–22646.

Talley, L.D., McCartney, M.S., 1982. Distribution and circulation of Labrador Sea-water. J. Phys. Oceanogr. 12 (11), 1189–1205.

Taylor, G.I., 1921. Diffusion by continuous movements. Proc. Lond. Math. Soc. 20, 196–212.

Taylor, G.I., 1953. Dispersion of soluble matter in solvent flowing slowly through a tube. Proc. R. Soc. Lond. A Math. Phys. Sci. 219 (1137), 186–203.

Taylor, G.I., 1954. The dispersion of matter in turbulent flow through a pipe. Proc. R. Soc. Lond. A Math. Phys. Sci. 223 (1155), 446–468.

Thompson, A.F., Young, W.R., 2007. Two-layer baroclinic eddy heat fluxes: zonal flows and energy balance. J. Atmos. Sci. 64, 3214–3231.

Treguier, A., 1999. Evaluating eddy mixing coefficients from eddy-resolving ocean models: a case study. J. Mar. Res. 57, 89–108.

Treguier, A.M., Held, I.M., Larichev, V.D., 1997. Parameterization of quasigeostrophic eddies in primitive equation ocean models. J. Phys. Oceanogr. 27, 567–580.

Treguier, A., Hogg, N., Maltrud, M., Speer, K., Thierry, V., 2003. The origin of deep zonal flows in the brazil basin. J. Phys. Oceanogr. 33, 580–599.

Tulloch, R., Marshall, J., Hill, C., Smith, K.S., 2011. Scales, growth rates, and spectral fluxes of baroclinic instability in the ocean. J. Phys. Oceanogr. 41 (6), 1057–1076.

Vallis, G.K., 2006. Atmospheric and Oceanic Fluid Dynamics: Fundamentals and Large-Scale Circulation. Cambridge University Press, Cambridge.

Veronis, G., 1975. The role of models in tracer studies. In: Numerical Models of Ocean Circulation: Proceedings of a Symposium Held at Durham, New Hampshire, October 17–20, 1972. National Academy of Sciences, pp. 133–146.

Visbeck, M., Marshall, J.C., Haine, T., Spall, M., 1997. Specification of eddy transfer coefficients in coarse resolution ocean circulation models. J. Phys. Oceanogr. 27, 381–402.

Wardle, R., Marshall, J., 2000. Representation of eddies in primitive equation models by a PV flux. J. Phys. Oceanogr. 30, 2481–2503.

Waterman, S., Jayne, S., 2011. Eddy-driven recirculations from a localized, transient forcing. J. Phys. Oceanogr. 42, 430–447.

Welander, P., 1959. An advective model of the ocean thermocline. Tellus 11 (3), 309–318.

Welander, P., 1971. The thermocline problem. Philos. Trans. R. Soc. Lond. A Math. Phys. Sci. 270, 415–421.

Wunsch, C., Stammer, D., 1995. The global frequency-wavenumber spectrum of oceanic variability estimated from TOPEX/POSEIDON altimetric measurements. J. Geophys. Res. 100 (C12), 24,895–24,910.

Young, W.R., 2010. Dynamic enthalpy, conservative temperature, and the seawater boussinesq approximation. J. Phys. Oceanogr. 40 (2), 394–400.

Young, W.R., 2012. An exact thickness-weighted average formulation of the boussinesq equations. J. Phys. Oceanogr. 42, 692–707.

Young, W.R., Jones, S., 1991. Shear dispersion. Phys. Fluids A Fluid Dynam. 3, 1087–1101.

Young, W.R., Rhines, P.B., Garrett, C.J.R., 1982. Shear-flow dispersion, internal waves and horizontal mixing in the ocean. J. Phys. Oceanogr. 12, 515–527.

Zhao, R., Vallis, G.K., 2008. Parameterizing mesoscale eddies with residual and Eulerian schemes, and a comparison with eddy-permitting models. Ocean Model. 23, 1–12.

Zhurbas, V., Oh, I., 2004. Drifter-derived maps of lateral diffusivity in the pacific and atlantic oceans in relation to surface circulation patterns. J. Geophys. Res. Oceans 109 (C5), C05015.

Zhurbas, V., Oh, I., Pyzhevich, M., 2003. Maps of horizontal diffusivity and Lagrangian scales in the Pacific Ocean obtained from drifter data. Oceanology 43 (5), 622–631.